Geochemistry Geophysics Geosystems G3
AN ELECTRONIC JOURNAL OF THE EARTH SCIENCES
Published by AGU and the Geochemical Society

Article
Volume 9, Number 4
26 April 2008
Q04036, doi:10.1029/2007GC001879
ISSN: 1525-2027

An integrated study of microstructural, geochemical, and seismic properties of the lithospheric mantle above the Kerguelen plume (Indian Ocean)

J. Bascou
UMR-CNRS 6524 "Magmas et Volcans," Université Jean Monnet, 23 Rue du Dr. P. Michelon, F-42023 St-Etienne, France (jerome.bascou@univ-st-etienne.fr)

G. Delpech
UMR-CNRS 8148, IDES, Université Paris Sud XI, Bâtiment 504, F-91405 Orsay, France

GEMOC ARC National Key Centre, Earth and Planetary Sciences, Macquarie University, New South Wales 2109, Australia

A. Vauchez
UMR-CNRS 5243, Géosciences Montpellier, Université Montpellier II, F-34095 Montpellier Cédex 5, France

B. N. Moine and J. Y. Cottin
UMR-CNRS 6524 "Magmas et Volcans," Université Jean Monnet, 23 Rue du Dr. P. Michelon, F-42023 St-Etienne, France

GEMOC ARC National Key Centre, Earth and Planetary Sciences, Macquarie University, New South Wales 2109, Australia

G. Barruol
UMR-CNRS 5243, Géosciences Montpellier, Université Montpellier II, F-34095 Montpellier Cédex 5, France

[1] Peridotite xenoliths brought up to the surface by the volcanism of the Kerguelen Islands represent a mantle that has been affected by a high degree of partial melting followed by intense melt percolation above the Kerguelen plume. These xenoliths are therefore particularly suitable to investigate effects of melt-rock interaction on crystallographic fabrics (lattice-preferred orientation (LPO)) of peridotite minerals and on the LPO-induced seismic properties of peridotites above a mantle plume. We have studied a suite of 16 ultramafic samples representative of different degrees of partial melting and magma-rock interaction among which the protogranular harzburgites are the least metasomatised xenoliths and dunites are the ultimate stage of metasomatism. Olivine LPO is characterized by high concentration of [010] axes perpendicular to the foliation and [100] axes close to the lineation or distributed in the foliation plane in harzburgites, whereas the high concentration of [100] axes is parallel to the lineation and [010] axes is perpendicular to the assumed foliation in dunites. Olivine LPO in harzburgites is interpreted as being due to a deformation regime in axial compression or transpression. The fabric strength of olivine decreases progressively from protogranular to poikilitic harzburgites and finally to dunites, for which it remains nevertheless significant (J index $\geq$ 3.8). Seismic properties calculated from LPO of minerals indicate that metasomatism at higher melt/rock ratio lowers the P wave velocities. The most significant difference between harzburgites and dunites corresponds to the distribution of S wave anisotropy. Harzburgites display the maximum of anisotropy within the foliation plane and the minimum of anisotropy perpendicular to the foliation plane, whereas the lowest anisotropy is parallel to the lineation for dunites.

These modifications of seismic properties as a result of metasomatic processes may induce seismic heterogeneities in the mantle above the Kerguelen plume. In addition, assuming a lithospheric mantle primarily harzburgitic and structured with a horizontal foliation, the seismic properties calculated for the Kerguelen xenoliths reconcile the rather high anisotropy evidenced by the horizontally propagating surface waves with the apparent isotropy revealed by the absence of splitting of vertically propagating teleseismic SKS waves recorded by the GEOSCOPE Kerguelen station.

Components: 11,697 words, 13 figures, 1 table.

Keywords: Kerguelen; mantle plume; seismic anisotropy; metasomatism; crystallographic fabric; lithosphere.

Index Terms: 8121 Tectonophysics: Dynamics: convection currents, and mantle plumes; 8030 Structural Geology: Microstructures; 7208 Seismology: Mantle (1212, 1213, 8124).

Received 30 October 2007; **Revised** 27 January 2008; **Accepted** 7 March 2008; **Published** 26 April 2008.

Bascou, J., G. Delpech, A. Vauchez, B. N. Moine, J. Y. Cottin, and G. Barruol (2008), An integrated study of microstructural, geochemical, and seismic properties of the lithospheric mantle above the Kerguelen plume (Indian Ocean), *Geochem. Geophys. Geosyst.*, *9*, Q04036, doi:10.1029/2007GC001879.

1. Introduction

[2] The Earth's upper mantle is seismically anisotropic. Studies of naturally and experimentally deformed samples [e.g., *Nicolas and Christensen*, 1987; *Mainprice et al.*, 2000] and numerical simulations [*Tommasi et al.*, 1999; *Kaminski*, 2006] demonstrate that the lattice-preferred orientation (LPO or crystallographic fabric) of olivine crystals induced by mantle flow is the main cause of the observed seismic anisotropy. During plastic deformation of peridotites, the [100] and [010] axes of olivine tend to be preferentially aligned parallel to the flow direction and normal to the flow plane, respectively, in accordance with the dominant activation of the (010)[100] slip system [e.g., *Nicolas and Poirier*, 1976]. Development of olivine LPO induces seismic anisotropy in the lithospheric mantle that may be further affected by reheating and melt percolation within the upper mantle. Although several studies have been devoted to examples of lithosphere-asthenosphere interactions [e.g., *Vauchez and Garrido*, 2001; *Tommasi et al.*, 2004; *Vauchez et al.*, 2005; *Le Roux et al.*, 2007], the effects of these processes on the fabric and the seismic properties of mantle rocks are still not fully understood.

[3] Recent petrophysical studies on peridotite samples suggest than the mineral LPO may be affected by heating and partial melting (asthenospherization) of the lithospheric mantle. For example, LPO measured in samples from the ''asthenospherized'' domain of the Ronda massif subcontinental lithospheric mantle show a weakening of the fabric strength [*Vauchez and Garrido*, 2001]. Moreover, variations in LPO symmetry with depth and the development of uncommon LPO patterns in xenoliths from the Labait volcano in the East African Rift suggest an increasing activity of the (010)[001] slip system [*Vauchez et al.*, 2005]. Regarding the oceanic lithospheric mantle, LPO patterns of minerals in peridotite xenoliths from the Southern Pacific [*Tommasi et al.*, 2004] appear little affected by melt percolation processes. The main variation of mineral LPO is a progressive weakening of the olivine LPO in dunites and wherlites in which static recrystallization occurred [*Tommasi et al.*, 2004]. On the other hand, experimental work on the deformation of partially molten mantle rocks under anhydrous conditions [*Holtzman et al.*, 2003] indicates that significant changes of olivine LPO may take place due to melt segregation and strain partitioning. However, the impact of this change on a regional-scale anisotropy is still discussed [*Kaminski*, 2006].

[4] In the last two decades, anisotropy, and particularly splitting of teleseismic shear waves such as the SKS waves, has been widely used to measure and constrain the active or frozen mantle flow and tectonic processes at depth [e.g., *Silver*, 1996]. Indeed, anisotropy may be related to mantle deformation since it results from strain-induced crystal preferred orientations [*Nicolas and Christensen*, 1987; *Babuska and Cara*, 1992]. Polarized shear waves (e.g., SKS, PKS...) traveling across a deformed mantle split in two orthogonal waves polarized in two orthogonal planes related to the strain fabric. These two split waves propagate through the anisotropic medium at different veloc-

ities that depend on the birefringence generated by the crystallographic fabric. This birefringence depends both on the arrangement and degree of the crystallographic axes concentration of the main minerals in the rocks. These two split shear waves are recorded at 3-components seismic stations and are classically characterized by the orientation (ϕ) of the fast S wave polarization plane, and the delay (δt) between the fast and slow split S wave arrivals.

[5] Whereas a large number of shear waves splitting measurements is available for various continental environments, the coverage is still sparse in oceanic environments. In the Indian Ocean, most of the oceanic stations have been described as isotropic [*Barruol and Hoffman*, 1999] except stations in the Seychelles [*Barruol and Ben Ismaïl*, 2001; *Hammond et al.*, 2005]. At the difference, shear wave splitting has been detected beneath most stations located in the Pacific Ocean [*Russo and Okal*, 1998; *Wolfe and Silver*, 1998; *Fontaine et al.*, 2007] except beneath Tahiti [*Fontaine et al.*, 2007] where two broadband and long-period permanent stations providing more than 15 years of data did not provide any evidence of SKS splitting. On the other hand, surface waves tomographies performed in the Indian Ocean [e.g., *Lévêque et al.*, 1998; *Debayle et al.*, 2005] or in the Pacific Ocean [*Montagner and Tanimoto*, 1991; *Maggi et al.*, 2006] suggest that both oceanic basins are pervasively anisotropic at both lithospheric and asthenospheric depth. To better understand why some oceanic domains are apparently isotropic for SKS waves and anisotropic for horizontally propagating surface waves, we performed a detailed study of the petrography, geochemistry and petrophysical characteristics of upper mantle rocks brought up to the surface by the Kerguelen volcanism. Indeed, more constraints are needed to discuss mantle processes and dynamics from seismic anisotropy observations.

[6] The Kerguelen Islands result from a particular geodynamic history above the long-lived Kerguelen plume. They started to form about 42 Ma ago when the Kerguelen plume was located beneath or near the South East Indian Ridge (SEIR), whereas it is currently in an intraplate position in the Antarctic plate [*Gautier et al.*, 1990; *Giret*, 1993] (Figure 1). Ultramafic xenoliths brought up to the surface by alkaline magmas of the Kerguelen Islands are predominantly spinel harzburgites and dunites. These rocks represent a lithospheric mantle that underwent a significant degree of partial melting followed by the percolation of large volumes of magma above the Kerguelen plume. The effects of mantle-melt interactions on the petrology and geochemistry of these xenoliths have been extensively studied [*Mattielli et al.*, 1996; *Grégoire et al.*, 1997, 2000a, 2000b; *Moine et al.*, 2001, 2004; *Delpech et al.*, 2004]. In this contribution, we combine microstructural analyses and seismic properties calculations with existing and new geochemical studies to investigate whether and how magma-peridotite interaction modifies seismic properties of the oceanic mantle. Sixteen ultramafic xenoliths having undergone various degrees of partial melting and metasomatism were selected for this study. This enables us to discuss the olivine LPO evolution, the impact on the seismic properties and the consequence on the interpretation of SKS splitting and surface wave anisotropic tomographies.

2. Sampling and Petrology

[7] Selected peridotite xenoliths come from various localities in the Kerguelen Archipelago (Figure 1) and display differences in structure, chemical and modal compositions (Table 1).

[8] Harzburgites show mainly protogranular and poikilitic structures [*Mercier and Nicolas*, 1975; *Coisy and Nicolas*, 1978] (Figure 2). However, some samples tend to develop a porphyroclastic structure with large olivine and orthopyroxene crystals (>2 mm) displaying undulose extinctions and subgrain boundaries. These porphyroclasts are surrounded by fine strain-free neoblasts. Protogranular harzburgites display olivine and orthopyroxene grains ranging from 2 to 10 mm in size. The grain boundaries are curvilinear, suggesting grain boundary migration and the largest grains of olivine and orthopyroxene commonly display evidence of plastic strain such as subgrain boundaries (Figures 2a–2c). Olivine grains in poikilitic harzburgites are large (up to 5 cm long) and contain inclusions of orthopyroxene. Clinopyroxene displays inclusions of resorbed orthopyroxene and spinel grains (Figure 2d). Few samples contain secondary minerals such as amphibole and phlogopite (see Table 1). In the various types of harzburgites vermicular grains of spinel occur between olivine and pyroxene grains and commonly form clusters with orthopyroxene and clinopyroxene. Sample JGM92-1c has 7% modal clinopyroxene and is a clinopyroxene-poor lherzolite (Table 1). It

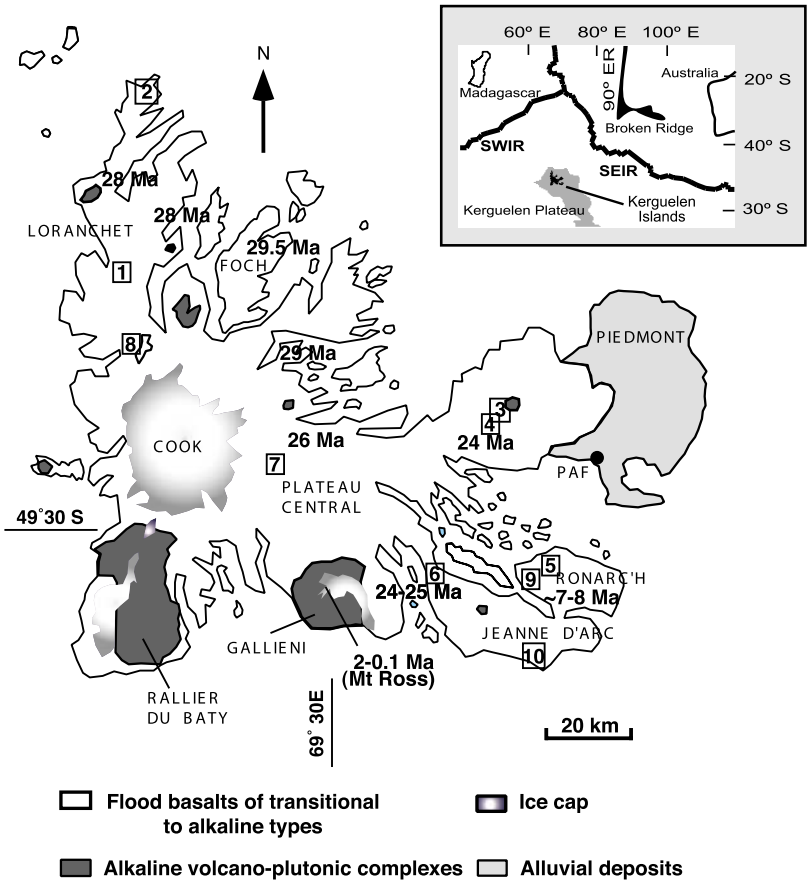

Figure 1. Location of dikes hosting xenoliths, modified after *Grégoire et al.* [1997]: 1, Lac Michèle (BY96-394, BY96-397); 2, Table de l'Oiseau (GR97-38); 3, Mont du Chateau (OB93-3, OB93-5); 4, Val Studer (OB93-58, JGM92-1c); 5, Trièdre (GM92-453, GM92-468); 6, Dôme Rouge (OB93-426, GM92-31); 7, Plateau Central (BOB93-640.1); 8, Vallée Ring (MM94-54, MM94-97); 9, Pointe de l'Espérance (GM92-214); 10, Mont Tizard (MG91-114). Geochronological data of flood basalts after *Nicolaysen et al.* [2000]. The Geoscope station of Kerguelen (PAF: −49.351°N, 70.213°E) is also plotted on this map.

has the same microstructural and geochemical characteristics as the poikilitic harzburgites [*Grégoire et al.*, 2000b] and will be hereafter included in the poikilitic harzburgite samples.

[9] Dunites display both unequigranular and equigranular structures (Figures 2e and 2f). Grain size for the unequigranular structure ranges from 1 to 6 mm (samples MG91-114, GM92-468). The largest grains are frequently slightly elongated and display evidence of plastic strain such as widely spaced subgrain boundaries. The smallest grains usually display a polygonal shape, without evidence of plastic deformation. Equigranular dunites (MG94-54, GM92-214, BOB93-640.1, MM94-97) display olivine grains 0.5 to 1 mm in diameter, free of internal strain and polygonal in shape with frequent 120° triple-point boundary. This equilibrated microstructure suggests static recrystallization through grain boundary migration. Isolated globular to anhedral grains of spinel are either interstitial or occur as inclusions in olivine. Secondary minerals such as clinopyroxene and phlogopite are commonly interstitial.

3. Geochemistry of the Mantle Xenolith Suite

[10] The petrography and geochemistry of eleven samples out of the sixteen used in the present paper have been previously studied by *Grégoire et al.* [2000a, 2000b], who also calculated equilibration temperatures. Data for the five remaining samples GR97-38, BY96-394, BY96-397, GM92-31 (harzburgites) and MG91-114 (dunite) have been obtained using similar analytical methods as those described by *Grégoire et al.* [2000a, 2000b]. Average major and trace element data for these samples can be found in auxiliary material Table S1.[1]

[1]Auxiliary materials are available at ftp://ftp.agu.org/apend/gc/2007gc001879.

Table 1. Petrography, Calculated Modal Composition, and Mg# and Cr# Numbers of Minerals for Mantle Xenoliths from the Kerguelen Islands[a]

Samples	OB93-426	OB93-58	GM92-31	GR97-38	BY96-397	OB93-3	OB93-5	JGM92-1c	GM92-453	BY96-394	MG91-114	GM92-468	MM94-54	GM92-214	BOB93-640.1	MM94-97
Location	6	4	6	2	1	3	3	4	5	1	10	5	8	9	7	8
Rock type	H	H	H	H	H	H	H	Lhz	H	H	D	D	D	D	D	D
Texture	Prot.	Prot.	Prot.	Prot.	Prot.	Poik.	Poik.	Poik.	Poik.	Poik.	Unequigr.	Unequigr.	Equigr.	Equigr.	Equigr.	Equigr.
Modal composition, %																
Olivine	71	79	76	75.5	72	66.5	74	79	86	79.5	97.5	95.85	95.1	90.3	94	98.15
Opx	26	19	21.5	20.5	25	29.3	21	13	11	19	0	-	-	1.5	-	-
Cpx	2.5	1.5	1.5	3.5	2.5	3.3	3.5	7	2.5	0.6	1.5	0.75	2.9	5.8	3.1	0.8
Spinel	0.5	0.5	1	0.5	0.5	0.6	0.5	1	0.5	0.9	1	3	1.6	2.5	2	1
Amphibole	-	-	-	-	-	+	0.5	-	-	-	-	-	-	-	-	-
Phlogopite	-	-	-	-	-	-	0.5	-	-	-	-	0.4	0.4	-	0.9	0.05
Carbonate	-	-	+	-	-	-	-	-	+	+	-	-	+	+	+	+
Plagioclase	-	-	-	-	+	-	-	-	-	+	-	-	-	-	-	-
Apatite	-	-	-	-	+	-	-	-	-	+	-	-	-	-	-	-
K-feldspar	-	-	-	-	-	-	+	-	-	-	-	-	-	-	-	-
Sum	100	100	100	100	100	99.7	100	100	100	100	100	100	100	100.1	100	100
Mg#(Ol)	91.5	91.7	91.4	91.5	90.3	91.3	91.5	86.6	89.8	91.2	87.2	89.8	86.8	88.7	86.1	87.5
Mg#(Opx)	92.3	92.5	91.9	92.2	91.2	91.8	91.9	87.5	90.2	92	-	-	-	89.6	-	-
Mg#(Cpx)	93.5	93.8	93.3	93.5	93.6	90.9	91.4	86.6	88.7	93.7	89.6	90.2	88.5	88.4	88.1	88.9
Mg#(Sp)	68.9	68.6	68.3	68.5	68.9	71.4	75.6	61.4	59.5	70	52.6	58.9	62.1	73.5	50.1	49.7
Cr#(Sp)	46.1	45.8	48.4	51.3	45.9	35.6	27.8	33.7	44.1	50.6	35.6	51.3	31.6	25	25	31.2

[a]H, harzburgite; Lhz, lherzolite; D, dunite; Prot., protogranular; Poik., poikilitic; Unequigr., unequigranular; Equigr., equigranular.

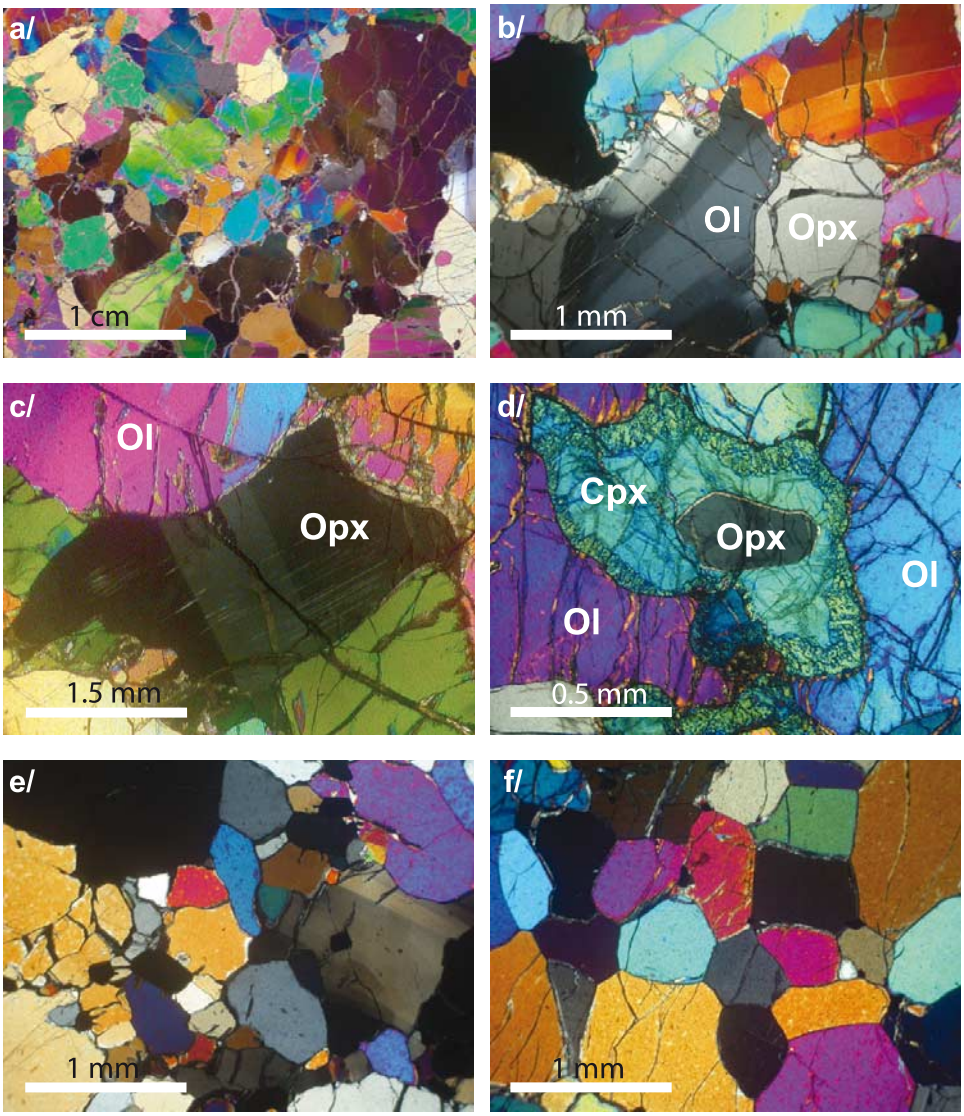

Figure 2. Photomicrographs (crossed polarizers) showing typical microstructures of the Kerguelen peridotite xenoliths. (a) Protogranular harzburgite GM92-31. (b and c) Details of olivine and orthopyroxene grains in protogranular harzburgite GM92-31. The grains display a well-developed substructure, which suggests dislocation-flow. (d) Poikilitic clinopyroxene with spongy rims interpreted as product of interaction between harzburgites and alkaline basaltic melt, courtesy of M. Grégoire. (e) Unequigranular dunite MG91-114. (f) Equigranular dunite MM94-97.

3.1. Mineral Chemistry

3.1.1. Major Elements

3.1.1.1. Protogranular Harzburgites

[11] Minerals (Ol, Opx, Cpx, Sp) from protogranular harzburgites (OB93-58, GM92-426, GM92-31, GR97-38 and BY97-397) have the highest Mg# (Mg# = 100 × MgO/(MgO + FeO_T)) and the lowest contents of basaltic components (Al, Na, Ti, Cr, Fe), Table 1 and Figure 3. The Mg# of olivine in the protogranular harzburgites varies between 91.4 and 91.7, except sample BY96-397 which has olivine with lower Mg# (90.3; Table 1 and Figure 3a). Clinopyroxene is a diopside characterized by high CaO, low Al_2O_3, TiO_2 and Na_2O contents (Figures 3b–3e) and spinel has high Cr# (Cr# = 100 × Cr/(Cr + Al)) ranging from 45 to 53 and high Mg# varying between 65.7 and 74.5 (Figure 3f). Compared to minerals in abyssal peridotites [*Dick*, 1989], which represent the composition of a typical oceanic lithosphere (without a plume influence), minerals in protogranular harzburgites have higher

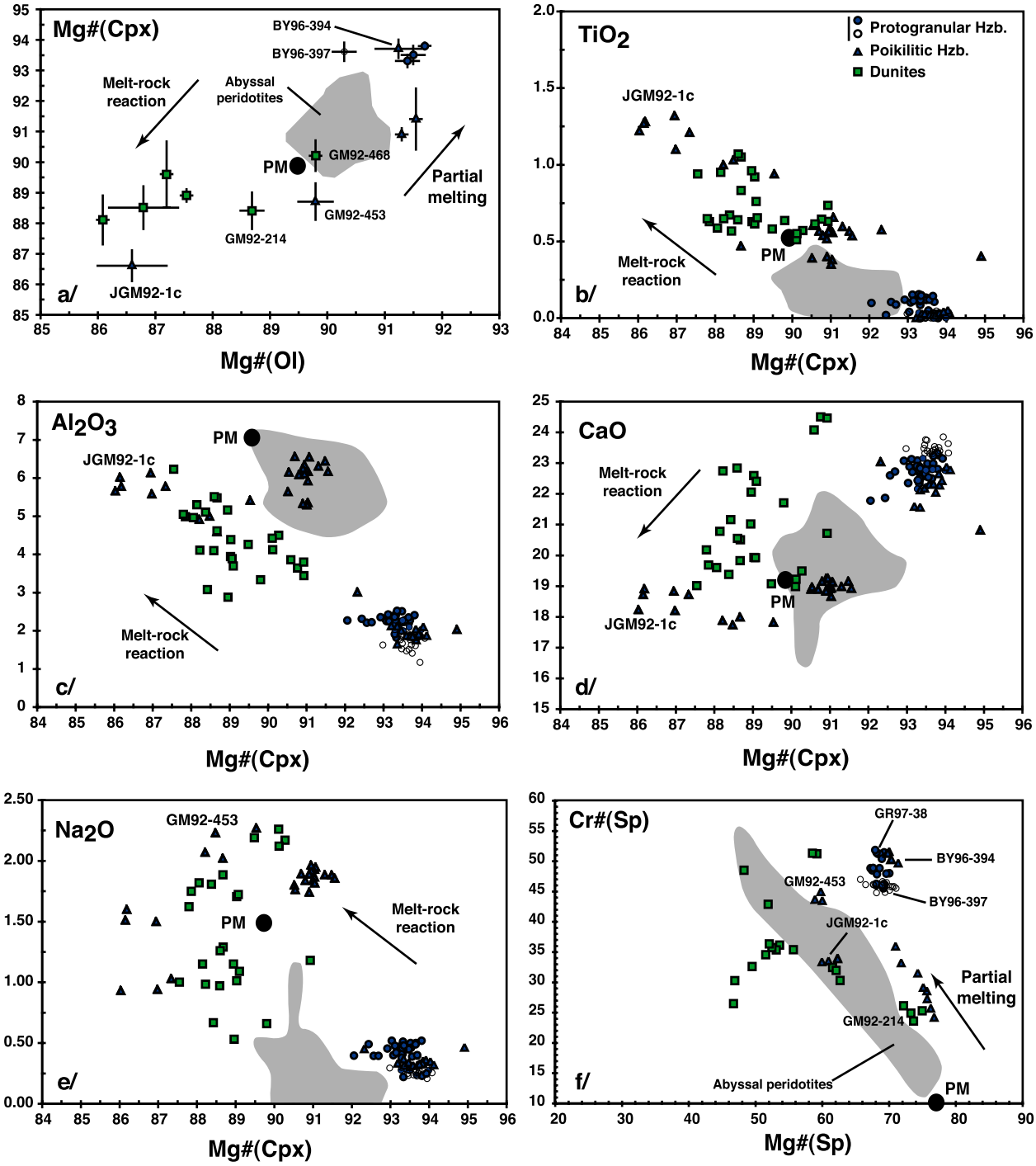

Figure 3. Major element compositions of minerals (olivine, spinel, clinopyroxene) in harzburgites and dunites from Kerguelen Islands. Grey field, abyssal peridotites after *Dick* [1989]; dark blue circles, protogranular harzburgites; empty circles, protogranular harzburgite BY96-397; dark blue triangles, poikilitic harzburgites; green squares, dunites. PM indicates the approximate composition of clinopyroxene and spinel of the Primitive Mantle. The arrows indicate the effect on the PM of progressive melt-rock reactions between the depleted protogranular harzburgites and percolating silicate melts (metasomatism) and the effect of partial melting. In Figure 3a the bars indicate the 1σ deviation for each sample analyzed. Typical %RSD (relative standard deviation) on the analyses of major elements by EMP (electron microprobe) are of the order of 0.3 for TiO_2, <0.3 for Al_2O_3, 0.4 for CaO, <0.9 for Na_2O, 0.3 for MgO, 0.5 for FeO, and 0.04 for Mg#. Uncertainties are smaller than symbol size.

Mg#, clinopyroxenes have lower contents of basaltic components and spinels higher Cr# for a given Mg#. Equilibration temperatures estimated from these samples range between 910 and 1000°C (see *Grégoire et al.* [2000a, 2000b] for details).

3.1.1.2. Poikilitic Harzburgites

[12] Samples OB93-3, OB93-5, JGM92-1c, GM92-453 and BY96-394 have minerals with lower Mg# than in protogranular harzburgites, except in sample BY96-394. They display very variable Mg# (and Cr# for spinels) compared to protogranular samples (Mg#(Ol) = 86.6–91.3; Mg#(Cpx) = 86.6–93.7; Cr#(Sp) = 27.8–44.1; Table 1 and Figure 3). Clinopyroxene is a magnesian augite that has higher contents of basaltic components (i.e., higher Al_2O_3, TiO_2, Cr_2O_3 and Na_2O contents and lower CaO contents) than the clinopyroxene in protogranular harzburgites (Figures 3b–3e). Although the sample BY96-394 displays microstructural characteristics of poikilitic harzburgites, the major element compositions are similar to those in protogranular harzburgites (Figure 3). Most spinels are also enriched in TiO_2 compared to protogranular samples (0.26–1.67 wt%; see *Grégoire et al.* [2000a, 2000b] for details). Equilibration temperatures estimated for these samples are higher than in protogranular harzburgites and range between 1015 and 1125°C.

3.1.1.3. Dunites

[13] Minerals in dunites (olivine, clinopyroxene, spinel) display Mg# that are in the range of those for olivine and clinopyroxene in poikilitic harzburgites (Table 1 and Figure 3). The Mg# in olivine displays a wide range of variation, from 89.8 in GM92-468 to more Fe-rich olivines in sample MM94-54 (Mg# = 86.8). Clinopyroxene is Mg-Al diopside with Mg# varying between 88.1 and 90.2 (Table 1) which has variable major element compositions between those of clinopyroxene in protogranular samples and those of the poikilitic samples (JGM91-1c, GM92-453; Figures 3b–3e). The decrease in Mg# is accompanied by an increase in basaltic components Al, Na, Ti and a decrease in Ca (Figure 3). Spinel is a magnesian chromite with a wide range of major element compositions in Mg# (49.7–73.5) and Cr# (25.0–51.3) (Figure 3f). Most dunites have spinels with Mg# lower than for harzburgites except in dunite GM92-214 (73.5, Table 1). However, the Cr# is highly variable and covers the range displayed by spinels in both types of harzburgites (Figure 3f). Equilibration temperatures estimated for dunites range between 940 and 1090°C (see *Grégoire et al.* [2000b] for details).

3.1.2. Trace Elements

3.1.2.1. Protogranular Harzburgites

[14] Trace element contents of clinopyroxenes in protogranular harzburgites are very low (Figure 4) compared to the primitive mantle estimate of *McDonough and Sun* [1995] and are highly variable between samples. Clinopyroxene in protogranular harzburgites displays a U-shaped pattern from Lu to La (Figure 4a). Clinopyroxenes in samples BY96-397 and GR97-38 have the lowest heavy rare earth element contents (HREE [Dy-Lu]; <1 × CI-Chondrite) and medium rare earth element contents (MREE [Sm-Gd]). These clinopyroxenes exhibit enrichments in the light rare earth elements (LREE [La-Nd]) and in the most incompatible elements (Rb, Th, U) but are less enriched in Ba, Nb, Sr, Zr, Ti compared to their neighboring elements.

3.1.2.2. Poikilitic Harzburgites

[15] Trace element contents of clinopyroxenes in poikilitic harzburgites are much higher and rather uniform compared to clinopyroxenes in protogranular samples (Figure 4), except sample BY96-394. Clinopyroxenes in poikilitic samples show a smooth enrichment from HREE to LREE with a peak at Nd (Figure 4b) and are enriched in the most incompatible elements (Rb, Ba, Th, U, Nb). They commonly have lower concentration of Pb, Zr, Hf and Ti than neighboring elements. Clinopyroxene in harzburgite BY96-394 has much lower trace element contents, similar to trace element concentrations in protogranular samples.

3.1.2.3. Dunites

[16] Clinopyroxenes in dunites have very variable trace element contents (Figure 4c). Clinopyroxene in dunite MG91-114 is depleted in LREE compared to MREE and HREE and it has the lowest LREE, MREE and Th, U contents. Clinopyroxene in the phlogopite-bearing dunite GM92-468 has a convex upward trace element pattern with a peak at Hf and has the highest REE contents (La-Lu) of the dunite xenolith suite. Other clinopyroxenes display trace element patterns with smooth enrichments from HREE to LREE (GM92-214, BOB93-640, MM94-54, MM94-97) and all are enriched in the most incompatible elements (Th, U, Ta, Sr ± Zr) but have lower concentrations of Rb, Ba, Nb ± Ta and Ti (Figure 4c). Clinopyroxenes in dunites GM92-468 and MM94-97 have trace element con-

centrations that are in the range of those of clinopyroxenes in poikilitic harzburgites.

3.2. Melt-Rock Reaction Processes in the Lithosphere Beneath the Kerguelen Archipelago

[17] In an olivine Mg# versus olivine modal % diagram (Figure 5) some protogranular harzburgites plot near the oceanic trend. This likely indicates that they represent residues of partial melting at relatively shallow depth in the spinel stability field [*Boyd*, 1989]. Some other harzburgites from Kerguelen Islands plot off this trend and show higher Mg# of olivine for low olivine modal abundances. This deviation from the oceanic trend and the enrichment in orthopyroxene of these harzburgites have been explained as a result of partial melting in the stability field of spinel although at a higher pressure under which, orthopyroxene is stable during melting (>1.5 GPa [*Hassler*, 1999]). In addition, the high Mg# of mineral phases (and Cr# for spinel, Table 1), the depletion in basaltic components (Al_2O_3, Na_2O, TiO_2, FeO; Figure 3) and the low HREE contents in clinopyroxenes (Figure 4) are characteristic features of a lithospheric mantle that has undergone extensive partial melting, close to exhaustion of clinopyroxene (>20% [*Grégoire et al.*, 1997, 2000b]). However, the enrichment in the most incompatible trace elements observed in clinopyroxene (Figure 4) suggests that the protogranular harzburgite suite has later experienced metasomatism by small amount of silicate melts without crystallizing new minerals ("cryptic" metasomatism).

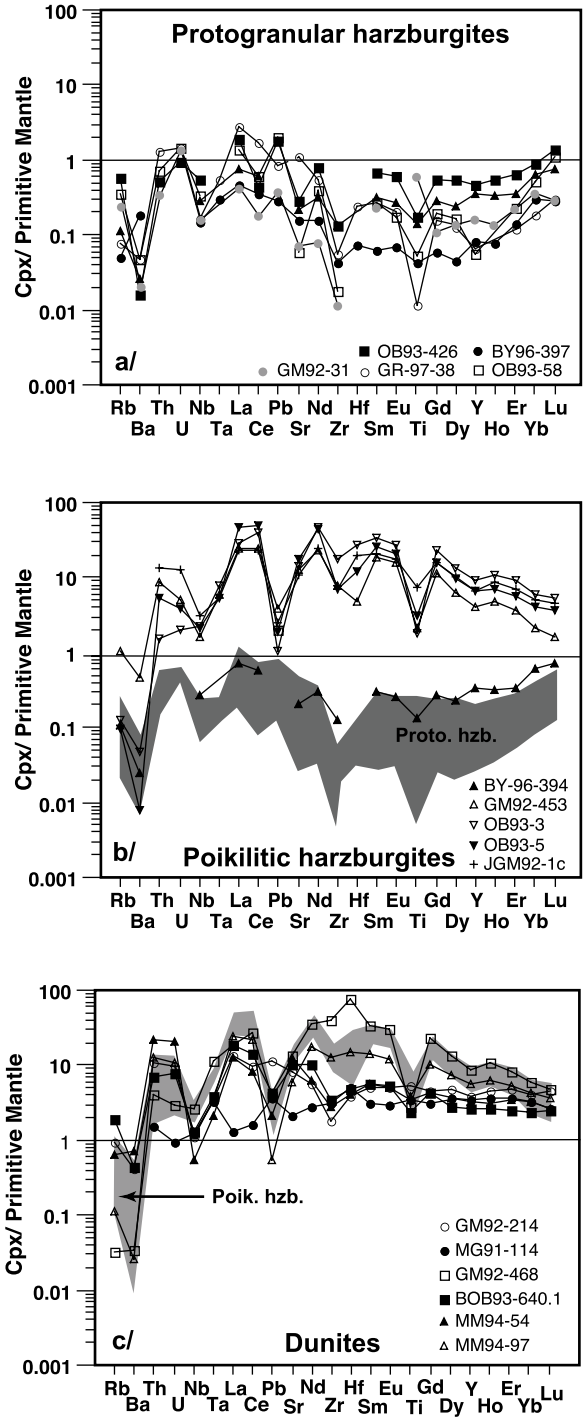

[18] In contrast, minerals in the poikilitic harzburgites are characterized by Mg# or Cr# similar or lower than in protogranular harzburgites. Clinopyroxene has higher contents of basaltic components (Al_2O_3, Na_2O, TiO_2; Figure 3) and it shows a global enrichment in the most incompatible elements. In Figure 5, most poikilitic harzburgites plot below the oceanic trend and display lower Mg# of olivine for higher olivine modal abundances. They also contain more clinopyroxene (2.5–7 wt%; Table 1) and minerals such as amphibole and more rarely phlogopite also occur in close association with clinopyroxene. This global enrichment in Fe, Al, Na, Ti, Cr (Figure 3) as well as in the most incompatible trace elements in clinopyroxene (Figure 4), and the crystallization of new minerals

Figure 4. Trace element concentrations in clinopyroxenes from (a and b) harzburgites and (c) dunites from Kerguelen Islands. Normalizing values for primitive mantle estimate after *McDonough and Sun* [1995]. Clinopyroxenes in protogranular harzburgites (Figure 4a) have low contents of trace elements compared to clinopyroxenes in poikilitic harzburgites (Figure 4b), which are enriched in the most incompatibles elements as a result of metasomatism at high melt/rock ratio. Clinopyroxenes in dunites have variable trace elements contents that attest to equilibration with heterogeneous silicate melts.

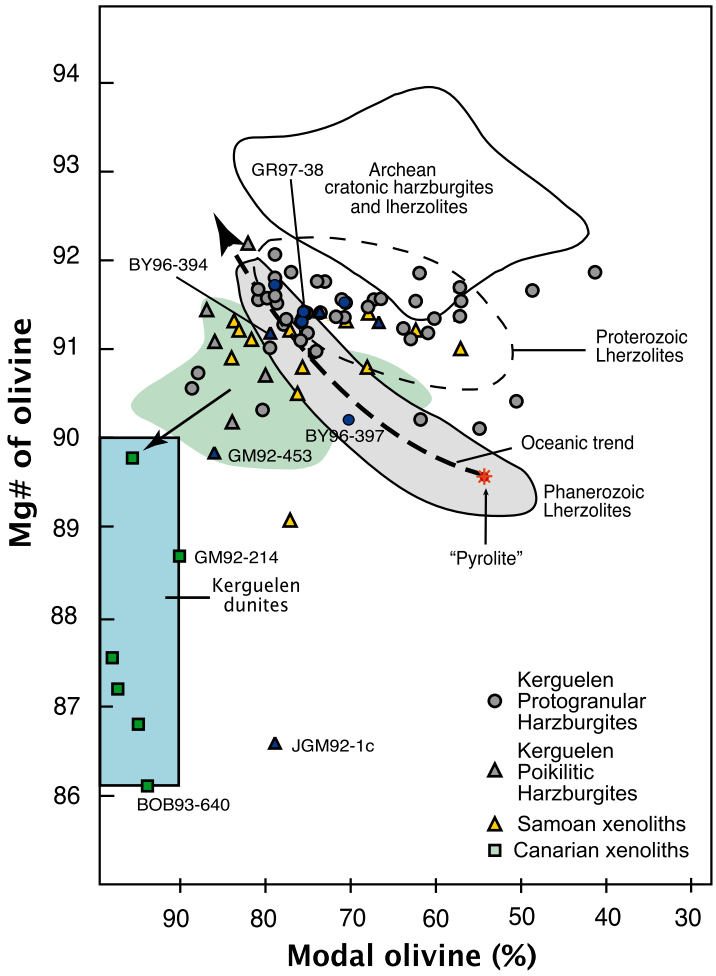

Figure 5. Mg# of olivine versus modal olivine for harzburgites and dunites from Kerguelen Islands after *Boyd* [1989]. Data for Kerguelen [*Hassler*, 1999; *Grégoire et al.*, 2000a, 2000b; this study]; Samoan xenoliths from *Hauri and Hart* [1994] and Canary Islands xenoliths from *Wulff-Pedersen et al.* [1996]. The dashed line represents the evolution of the Mg# of olivine and the olivine modal content of a peridotite undergoing progressive partial melting at relatively shallow depth in the lithosphere (<1.5 GPa [*Boyd*, 1989]).

(amphibole, phlogopite) are the consequences of modal metasomatism (i.e., metasomatism at high melt/rock ratio) into the depleted (protogranular) harzburgites and mafic alkaline silicate melts from the Kerguelen plume [*Grégoire et al.*, 2000b]. This metasomatic event resulted in a global re-enrichment in basaltic components and incompatible elements of the initially depleted lithospheric mantle beneath the Kerguelen Archipelago, at least in the vicinity of major melt pathways to the surface. The reaction between depleted (protogranular) peridotite and mafic alkaline silicate melts essentially led to the dissolution of orthopyroxene in the protogranular samples and crystallization of olivine and clinopyroxene (±volatile-bearing minerals) in poikilitic harzburgites. The ultimate end product of this metasomatic process at high melt/rock ratio is the formation of clinopyroxene-bearing dunite bodies with low Mg# of olivine as shown in Figure 5. These dunites derive from former harzburgites in which all the orthopyroxene was consumed during melt-rock reactions. Dunites sometimes contain volatile-bearing minerals (amphibole, phlogopite, Table 1). These minerals have likely crystallized from volatile and alkali-enriched silicate melt fractions at the end of the melt-rock reaction process. A secondary mineralogy (carbonate, plagioclase, K-feldspar, apatite) is sometimes observed in harzburgites and dunites as veins crosscutting the primary mineralogy or as reaction zones (Table 1). They correspond to late-stage metasomatic events that occurred shortly before eruption and that are

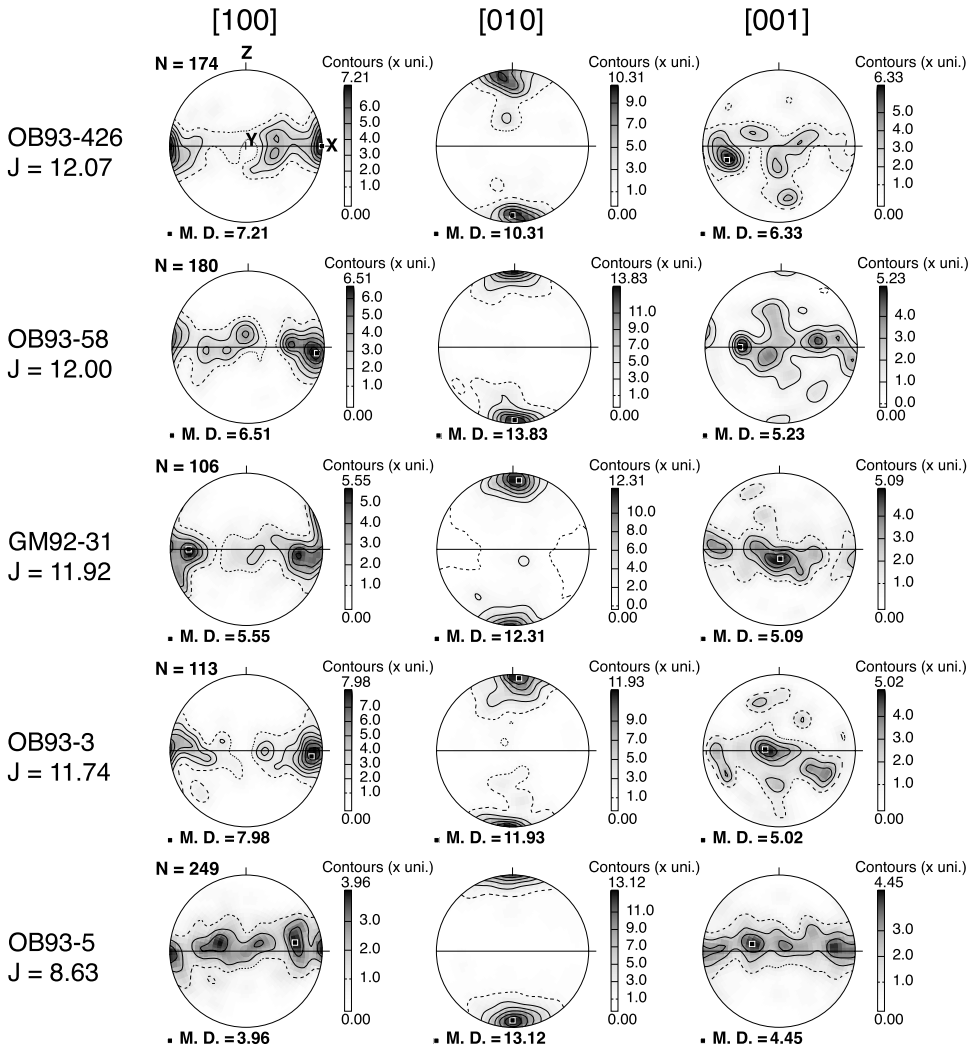

Figure 6. Olivine LPO in harzburgites. Equal area, lower hemisphere projections. Assumed foliation (XY plane) is marked by a black line, and lineation (X) is horizontal in the foliation plane; relationship between structural and crystallographic fabric is detailed in the text. N is the number of measurements. The density contours are in Multiple Uniform Distribution (MUD); M.D. is the maximum of density. The olivine fabric strength is given by the J index number.

related to metasomatism by small volumes of evolved melts through repeated reactions with the lithospheric mantle [*Grégoire et al.*, 1997; *Moine et al.*, 2004; *Delpech et al.*, 2004].

4. Lattice-Preferred Orientation

[19] Crystallographic orientation data were obtained by indexation of Electron Backscattered Diffraction patterns (EBSD technique) generated in the JEOL 5600 Scanning Electron Microscope (SEM-EBSD, Geosciences-Montpellier, France). Indexation of the observed patterns of Kikuchi bands was performed through a comparison with diffraction predicted for the analyzed crystal using the HKL CHANNEL 5+ software [*Schmidt and Olesen*, 1989]. The relative precision of crystal orientations measured from electron backscattering patterns is better than 1° [*Krieger Lassen*, 1996]. For all samples, the whole surface of the thin sections was investigated. The crystallographic orientation of minerals was measured following a grain-by-grain, operator-controlled indexing procedure to avoid possible bias due to oversampling of the largest grains and pseudo symmetry of olivine.

[20] Since the studied xenoliths are harzburgites and dunites, the LPO of olivine and orthopyroxene only has been measured (Figures 6–9). The fabric strength of olivine was calculated and expressed by the dimensionless texture J index [*Bunge*, 1982],

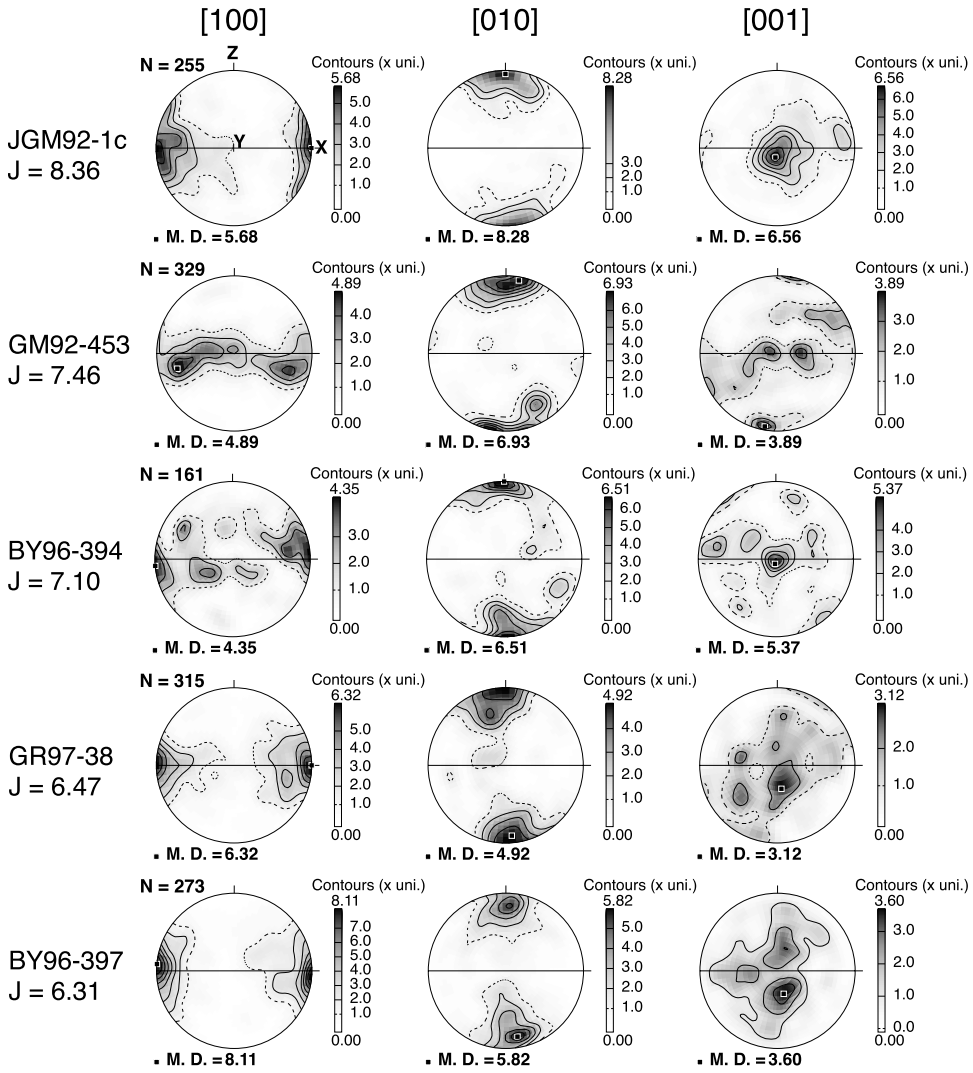

Figure 6. (continued)

which equals unity for a random distribution and tends toward infinity for a single crystal. *Ben Ismaïl and Mainprice* [1998] have shown that the fabric strength of olivine becomes stable from 100 measured grains. In this study, the minimum number of measurements for olivine is N = 106 (GM92-31) due to the large size of crystals (pluri-millimetric). The average number of measurements for olivine is N = 253.

4.1. Crystallographic and Structural Fabrics

[21] In most xenoliths, the foliation (XY structural plane) and lineation (X structural axis) are not easy to observe. In the studied harzburgites, a tight correlation is observed between the olivine [100] and the orthopyroxene [001] axes and between the olivine [010] and the orthopyroxene [100] axes, respectively. Dislocation creep in orthopyroxene occurs through dominant activation of the (100)[001] slip system, the most common slip system observed in naturally and experimentally deformed orthopyroxene [e.g., *Nazé et al.*, 1987]. During plastic deformation, the orthopyroxene [001] and [100] axes therefore tend to parallel the lineation and the pole of the foliation, respectively. The good correlation of olivine and orthopyroxene crystallographic axes suggests that olivine deformed through dislocation creep with (010)[100] as the dominantly activated slip system. The [100] and [010] olivine axes are thus considered as good proxies of the lineation direction (X axes) and foliation pole (Z axes), respectively [e.g., *Ben Ismaïl and Mainprice*, 1998]. Therefore to make comparison of the fabrics easier, LPO were oriented homogeneously to place the maximum concentration of olivine [100] and [010] axes, respectively, in

a horizontal EW and NS position and these orientations were labeled X and Z (Figures 6 and 9). In the dunites, constrains on the crystallographic and structural fabrics relationships provided by the orthopyroxene LPO are missing and we have considered that olivine LPO in dunites resulted from plastic deformation mechanisms and dominant activation of (010)[100] slip system, as in harzburgites. Olivine LPO in dunites as therefore been rotated in the same way as in harzburgites. It is noticeable than in the dunite MG91-114 where the foliation is relatively well marked by the shape-preferred orientation of minerals (olivine and spinel grains) a correlation between the [010] axes of olivine and the apparent pole of the foliation plane (Z) is observed.

4.2. Olivine Crystallographic Fabric

[22] LPO of olivine in harzburgites is characterized by a J index value ranging from 6.31 to 12.07 (Figure 6). Olivine LPO with medium to high J index value (J index > 7) systematically displays a [010]-fiber type pattern, according to the *Bunge*'s [1982] classification. This pattern is characterized by a stronger clustering of [010] axes relative to the other crystallographic axes. The [100] axes tend to form a girdle in the plane normal to the [010] maximum concentration (likely the foliation plane), with a maximum density assumed parallel the lineation. The [001] axes are more scattered than the [100] axes (except sample BY96-394) but they also usually display a girdle distribution in the foliation plane. In contrast, olivine LPO with weaker J index value (J index < 7) displays an orthorhombic LPO pattern characterized by a stronger clustering of [100] axes relative to [010] and [001] axes, which are the most scattered.

[23] LPO of olivine in dunites are characterized by lower J index values ranging from 3.80 to 6.99 and thus lower that the J index calculated for the olivine LPO in harzburgites (Figure 7). LPO pattern characterized by J index larger than 5 displays a stronger clustering of the [100] axes relative to the other crystallographic axes. The [010] axes tend to form a girdle perpendicular to [100], and the [001] axes are clustered close to the "Y" structural axis. The maximum density value (MD) of [010] and [001] axes are comparable (mainly from 4 to 5.7). LPO patterns of samples with the lower J index (BOB93-640.1 and MM94-97) are orthorhombic with a MD slightly higher for [010] than for [100] and [001].

[24] Figure 8 shows the P (point), G (girdle), and R (random) fabric components defined from the eigenvalue analysis formulated by *Vollmer* [1990]. We observe that the olivine [100] and [010] axes of protogranular harzburgites with high J index value (higher than 11) and dunites define two distinct groups. Contrarily, the poikilitic and protogranular harzburgites with lower J index value (<7, samples BY96-397 and GR97-38) are relatively scattered (around the protogranular harzburgite with high J index value and dunite group).

4.3. Orthopyroxene Crystallographic Fabric

[25] For orthopyroxene, it was not always possible to measure a large enough number of grains and we have therefore not calculated its J index. However, the orthopyroxene fabric pattern is well defined even if the number of grains is low (for example, sample OB93-3, N = 32; Figure 9). Orthopyroxene LPO is characterized by a strong clustering of [100] and [001] axes. This LPO is accounted by the dominant activation of (100)[001], which is the easiest and the most common slip system observed in naturally and experimentally deformed orthopyroxene [*Nazé et al.*, 1987]. Interestingly, most samples display a significantly higher concentration of [100] axes than of the other axes and a tendency for the [001] axes to have a girdle distribution. Thus, orthopyroxene and olivine LPO appear symmetrical compared to the structural frame, with the highest concentration of crystallographic axes perpendicular to the foliation.

5. Seismic Properties

[26] Seismic properties of the studied harzburgites and dunites were computed from single crystal elastic stiffness matrix, crystal orientation and density via the Christoffel equation [*Crosson and Lin*, 1971] using the *Mainprice* [1990] software. Input parameters are as follows: (1) the readjusted modal compositions of Table 1 ignoring the contribution of phlogopite, amphibole (present as accessory components, < 1%) and alteration minerals (e.g., serpentine), (2) the EBSD-measured LPO of major minerals (olivine and orthopyroxene), and (3) the elastic stiffness matrix of olivine, orthopyroxene, clinopyroxene and spinel using a Voigt-Reuss-Hill average [*Mainprice et al.*, 2000, and references therein]. The single crystal elastic constants and density data are taken from studies on olivine [*Abramson et al.*, 1997], enstatite [*Duffy and Vaughan*, 1988], diopside [*Collins and Brown*,

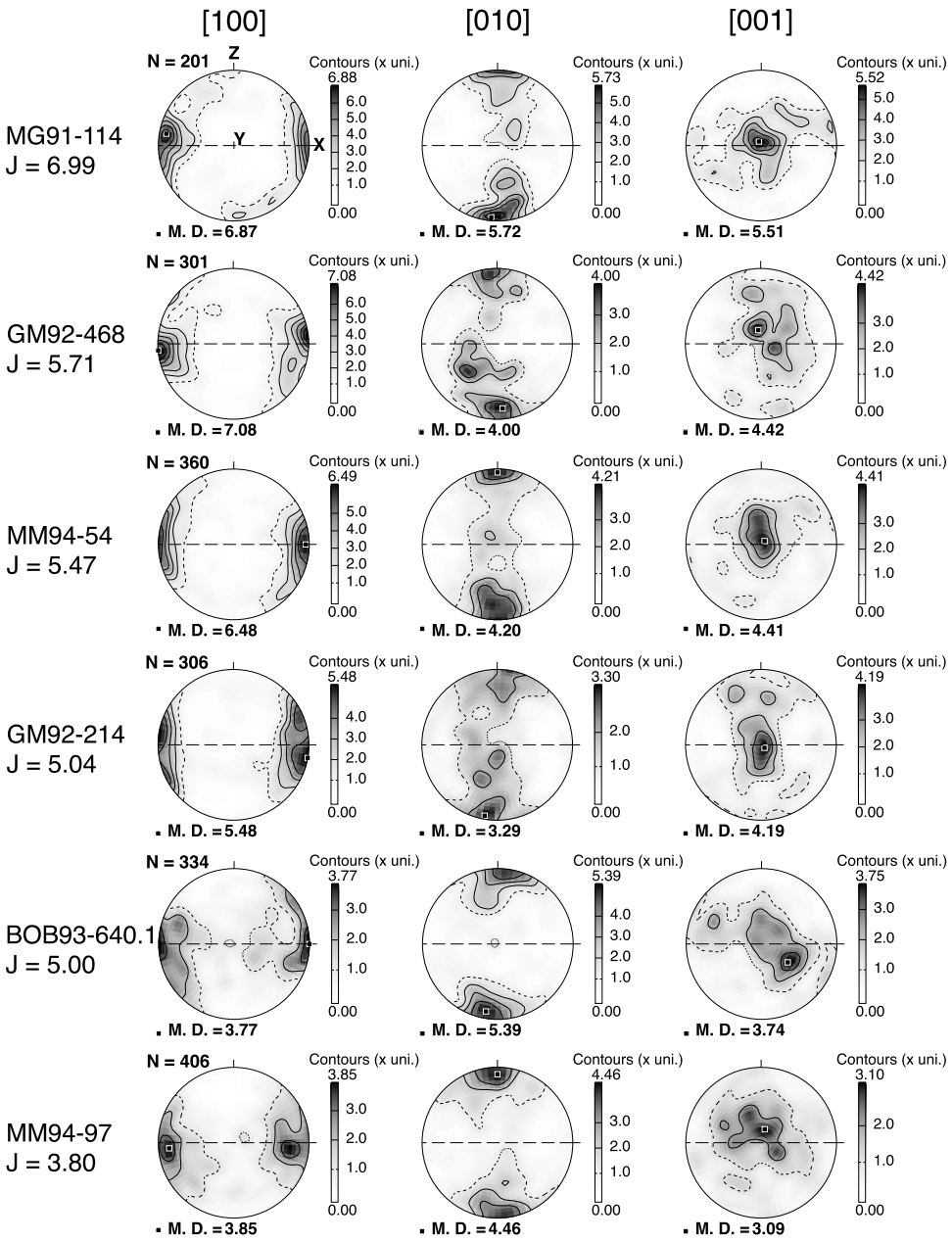

Figure 7. Olivine LPO in dunites. Equal area, lower hemisphere projections. Assumed foliation (XY plane) is marked by a dotted line and lineation (X) is horizontal in the foliation plane; relationship between structural and crystallographic fabric is detailed in the text. N is the number of measurements. The density contours are in Multiple Uniform Distribution (MUD); M.D. is the maximum of density. The J index number gives the olivine fabric strength.

1998] and spinel [*Li et al.*, 1995]. Due to the lack of statistically reliable LPO measurements for clinopyroxene and spinel we used the calculated isotropic elastic stiffness matrix of these minerals. In addition, the elastic stiffness matrix and the density of olivine were recalculated in order to take into account the variation of the forsterite content. 3-D seismic body waves velocity and azimuthal and polarization anisotropy are presented in a lower hemisphere projection and structural reference frame (Figures 10 and 11).

[27] Seismic properties of harzburgites displaying olivine [010]-fiber type LPO with medium and high J index value (J index > 7) and well-defined orthopyroxene LPO pattern show rather similar seismic properties (Figure 10a). Vp_{max} ranges from 8.48 to 8.66 km/s and Vp_{min} ranges from 7.90 to 8.06 km/s, resulting in a quite strong azimuthal

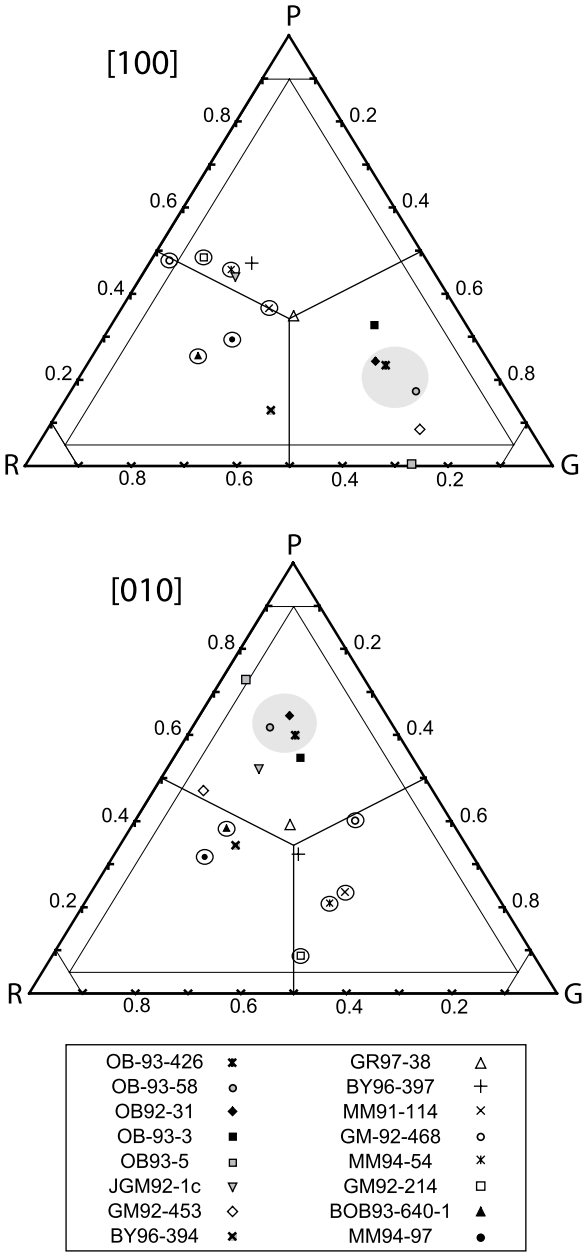

Figure 8. Eigenvalues analysis. Olivine LPO of each sample is plotted in a triangular diagram according to the P (point), G (girdle), and R (random) indexes of the distribution of the [100] and [010] crystallographic axes. Protogranular harzburgites with high J index values (higher than 11) are plotted in the gray zone, and dunites are in the circles.

anisotropy ranging from 5 to 9.2%. The fast velocities of P waves are either parallel to the maximum concentration of [100] (lineation) or distributed in the foliation and Vp_{min} is perpendicular to the foliation plane. The highest values of birefringence (AVs) range from 4.29 to 7.63% and are located in the foliation plane. The lowest are close to the maximum concentration of the [010] axis of olivine (pole of the foliation, Z). The fast split shear wave is polarized in a plane defined by the propagation direction and the maximum of olivine [001] (lineation). To better enhance the first-order characteristics of harzburgites from the Kerguelen mantle, we calculated an average harzburgite using samples OB93-426, OB93-58, OB92-31, OB93-3, OB-93-5, GM96-394 (Figure 10b). Averaging the seismic properties by giving the same weight to each sample is an interesting way to integrate the small-scale variations in composition and in microstructures, in a similar way to seismic waves. The average seismic properties are determined from calculation of the mean density and the 6x6 matrix coefficients of the stiffness tensor Cij describing the average elastic properties of the harzburgite samples (Figure 10b). The average harzburgite shows fast P wave parallel to the lineation and high P wave anisotropy (7%). The minimum of S wave polarization anisotropy (AVs) is ~0.2% (quasi isotropy) for a direction orthogonal to the foliation and the maximum of S wave anisotropy forms a girdle in the foliation with a maximum close to the *Y* axis. The maximum of S wave azimuthal anisotropy is higher than 2% (AVs1 = 4.8%, AVs2 = 2.8%).

[28] Most dunite samples are characterized by a stronger clustering of the olivine [100] axes and a distribution of [010] axes in a plane normal to the [100] axes. They display consistent seismic properties for P and S waves that differ from the properties of harzburgites described above particularly for S waves. The fast velocities of P waves are always parallel to the lineation and the slowest velocities form a girdle perpendicular to the [100] maximum of concentration and thus to the assumed foliation (Figure 11a). Vp_{max} ranges from 8.86 to 8.91 km/s and Vp_{min} ranges from 8.00 to 8.10 km/s resulting in a high azimuthal anisotropy (AVp > 8%). Seismic anisotropy of S waves is strong: AVs ranges from ~6 to ~7%. The highest values of AVs tend to form a girdle perpendicular to the [100] axes (flow direction) with a maximum close to [010] (i.e., normal to the assumed foliation plane) and the slowest anisotropy tends to parallel the lineation. The Vs1 polarization planes are colinear around the lineation, i.e., they are defined by the maximum concentration of [100] (the "X" structural axis) and the direction of propagation of the incoming S wave. An average dunite sample calculated using the data from samples MG91-114, GM92-468, MM94-54 and GM92-214 is shown Figure 11b. It is characterized by a high P wave

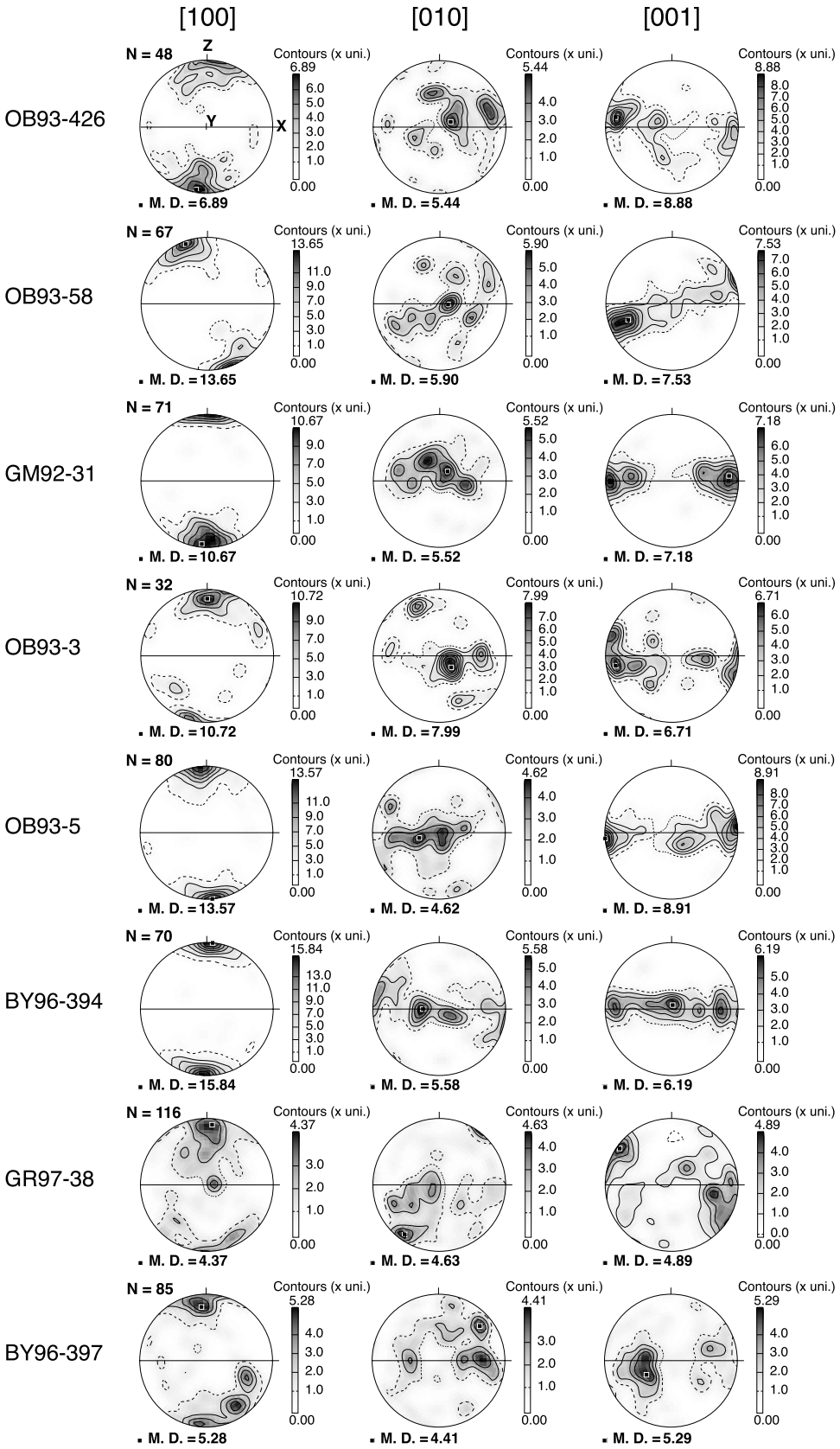

Figure 9. Orthopyroxene LPO in harzburgites. Projections and symbols for structural and crystallographic fabrics are similar to those in Figure 7.

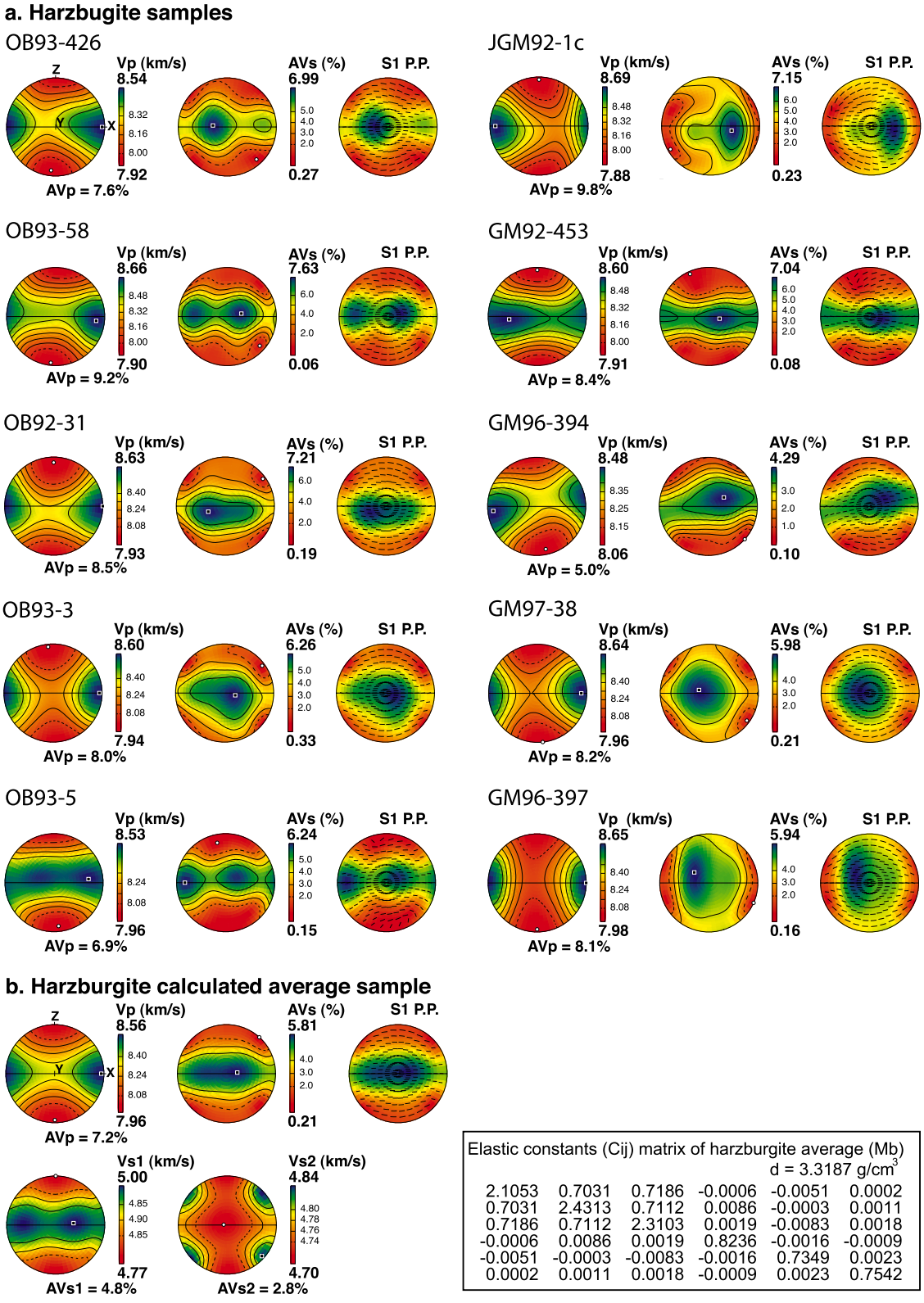

Elastic constants (Cij) matrix of harzburgite average (Mb)
d = 3.3187 g/cm^3

2.1053	0.7031	0.7186	-0.0006	-0.0051	0.0002
0.7031	2.4313	0.7112	0.0086	-0.0003	0.0011
0.7186	0.7112	2.3103	0.0019	-0.0083	0.0018
-0.0006	0.0086	0.0019	0.8236	-0.0016	-0.0009
-0.0051	-0.0003	-0.0083	-0.0016	0.7349	0.0023
0.0002	0.0011	0.0018	-0.0009	0.0023	0.7542

Figure 10

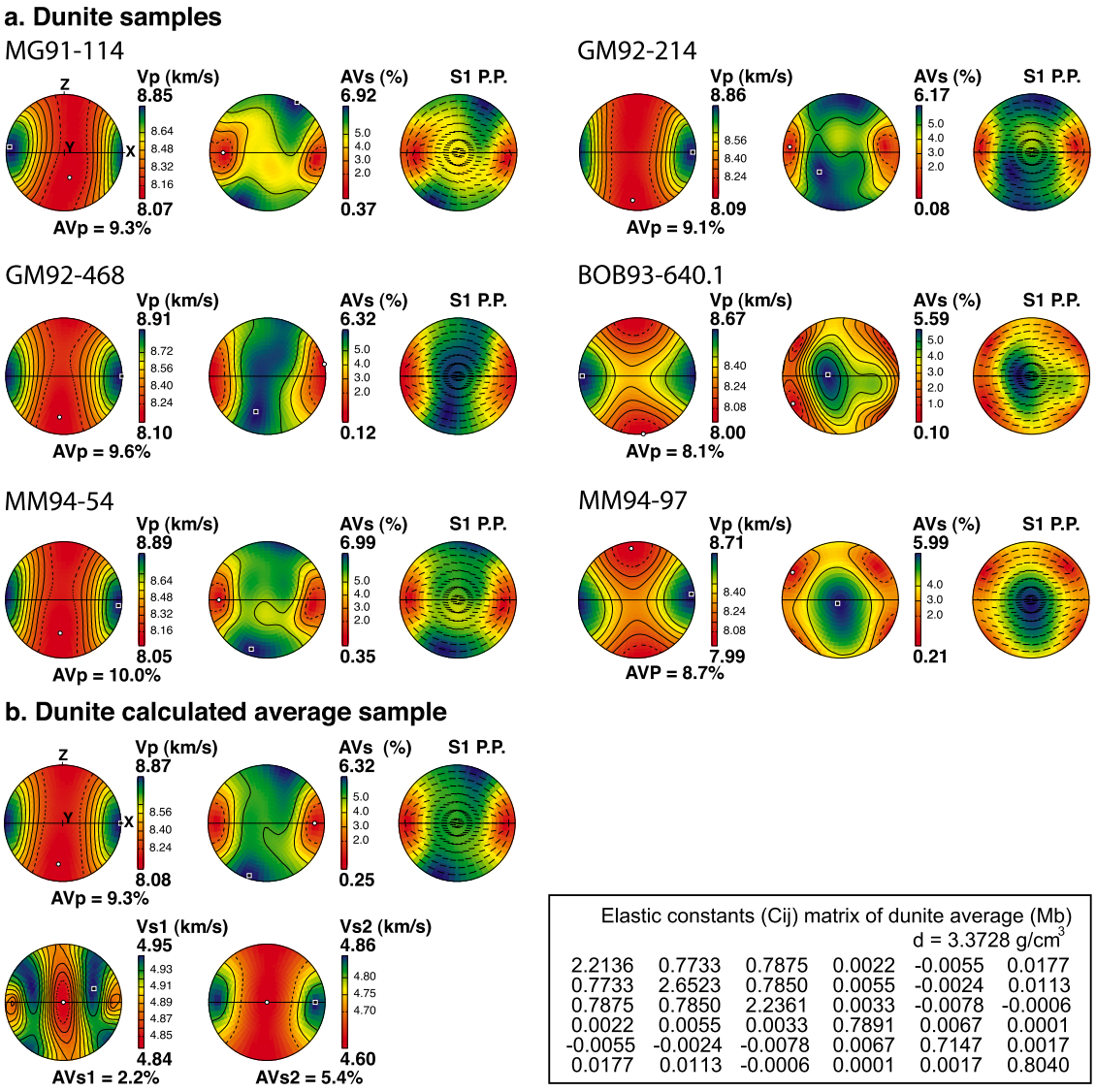

Elastic constants (Cij) matrix of dunite average (Mb)
d = 3.3728 g/cm^3

2.2136	0.7733	0.7875	0.0022	-0.0055	0.0177
0.7733	2.6523	0.7850	0.0055	-0.0024	0.0113
0.7875	0.7850	2.2361	0.0033	-0.0078	-0.0006
0.0022	0.0055	0.0033	0.7891	0.0067	0.0001
-0.0055	-0.0024	-0.0078	0.0067	0.7147	0.0017
0.0177	0.0113	-0.0006	0.0001	0.0017	0.8040

Figure 11. Calculated seismic properties of Kerguelen dunites. Data are presented in an equal area lower hemisphere projection; reference frame as in Figure 7. Vp (km/s), P wave velocity; AVp (%), anisotropy of P waves defined as $100 \times [(Vp_{max}-Vp_{min})/((Vp_{max}+Vp_{min})/2)]$; AVs (%), polarization anisotropy of S waves defined for a specific direction as $100 \times [(Vs_1 - Vs_2)/[(Vs_1 + Vs_2)/2)]$, where Vs_1 and Vs_2 are the fast and slow S wave velocities, respectively; S_1 P.P., polarization plane of the fast shear wave (S_1) as a function of the orientation of the incoming wave relative to the foliation (XY plane, full line) and lineation (X). Maximum and minimum values are shown on the plots as black squares and white spots, respectively.

anisotropy (9%) and by a girdle of high S wave anisotropic directions normal to the lineation with a maximum perpendicular to the foliation and a minimum parallel to the lineation. The maximum of S wave azimuthal anisotropy is higher than 4% (AVs1 = 4.95%, AVs2 = 5.4%).

[29] Seismic properties computed for harzburgites GM97-38 and GM96-397 and dunites BOB93-

Figure 10. Calculated seismic properties of Kerguelen harzburgites. Data are presented in an equal area lower hemisphere projection. Reference frame as in Figure 6. Vp (km/s), P wave velocity; AVp (%), anisotropy of P waves defined as $100 \times [(Vp_{max} - Vp_{min})/((Vp_{max} + Vp_{min})/2)]$; AVs (%), polarization anisotropy of S waves defined for a specific direction as $100 \times [(Vs_1 - Vs_2)/[(Vs_1 + Vs_2)/2)]$, where Vs_1 and Vs_2 are the fast and slow S wave velocities, respectively; S_1 P.P., polarization plane of the fast shear wave (S_1) as a function of the orientation of the incoming wave relative to the foliation (XY plane, full line) and lineation (X). Maximum and minimum values are shown on the plots as black squares and white spots, respectively.

640.1 and MM94-97 are rather similar and show differences with those of harzburgites and dunites mentioned above. The P wave velocity pattern is orthorhombic with Vp_{max} parallel to the lineation and Vp_{min} perpendicular to the foliation. Vp_{max} ranges from 8.64 to 8.71 km/s and Vp_{min} from 7.96 to 8.00 km/s, resulting in a Vp anisotropy (AVp) of 8.1 to 8.7%. AVs ranges from ~5.6 to 6% with the highest anisotropy close to Y (i.e., normal to both [100] and [010] maximum of concentration) and the lowest anisotropies perpendicular to the foliation pole and close to the lineation. As for the dominant harzburgite and dunite types, Vs1 is polarized in a plane that contains the propagation direction and the lineation. These properties are intermediate between those of the samples displaying an olivine [010]-fiber pattern (Figure 10b) and to the samples displaying a stronger clustering of the olivine [100] axes (Figure 11b). For the two dunites BOB93-640.1 and MM94-97, the change in LPO and seismic properties pattern is correlated to the decrease of olivine fabric strength due to static recrystallization.

6. Discussion

[30] The Kerguelen Islands represent the apex of the northern part of the Kerguelen-Heard oceanic plateau, the second largest oceanic plateau in the world [*Coffin and Eldhom*, 1994]. It results from a geodynamic context that evolved from continental rifting (125–100 Ma ago) to a stage during which an oceanic ridge formed above a mantle plume (around 42 Ma) and finally to an intraplate hot spot-mantle plume location [*Giret*, 1993; *Duncan*, 2002]. Metasomatism resulting from magma percolation above the Kerguelen plume affects a strongly deformed and structured mantle as supported by microstructural observations, LPO measurements and fabric strength values in protogranular harzburgites. The presence of spinel in the harzburgite xenolith suite together with the thermobarometric estimates [*Grégoire et al.*, 2000b] indicate a mantle slice between 30 and 70 km in depth. Protogranular harzburgites represent the part of the mantle the least affected by magma-rock interactions as indicated by geochemical data. These rocks have only experienced incipient metasomatism by small melt volumes, which resulted in enrichment of clinopyroxene in the most incompatible elements. Metasomatism at higher melt/rock ratio is accompanied by the development of a poikilitic structure in the harzburgites. From a mineralogical point of view, the reaction between harzburgites and silicate melt leads to dissolution of orthopyroxene and crystallization of olivine, and ultimately produces dunites when all the orthopyroxene has reacted out. Dunites represent therefore a former harzburgitic mantle, which reacted with large volumes of silicate melts. Dunite bodies likely represent a limited volume of mantle rocks located along and close to melt pathways or localized near the crust-mantle boundary where melts may segregate and react with the uppermost lithospheric mantle [*Grégoire et al.*, 1997].

6.1. Significance of LPO Patterns in Harzburgites

[31] Harzburgites display olivine LPO pattern of [010]-fiber type characterized by the dispersion of [100] and [001] within a plane orthogonal to the maximum concentration of [010] (foliation plane). The interpretation of this LPO is still not fully understood. Two main types of causes have been suggested to explain its development: a departure from simple shear and an increasing activity of the (010)[001] slip system during deformation.

[32] From numerical modeling of LPO development due to various strain regimes, *Tommasi et al.* [1999] have shown that [010]-fiber LPO pattern may develop under mantle conditions of transpression and axial compression. This LPO pattern in such case, results from the activation of the high temperature (010)[100] slip system and the dispersion of the [100] axes is due to the compressional component.

[33] From experiments, *Jung and Karato* [2001] have suggested that the (010)[001] slip system may become dominant for dislocation creep under high water content and/or high stress (or strain rate) conditions, resulting in a LPO (“B-type”) characterized by a concentration of [001] and [010], respectively, close to the lineation and the pole of the foliation plane. According to *Holtzman et al.* [2003] this LPO may also be a result of strain partitioning associated to melt segregation. Activation of the (010)[001] slip system may also result from a change in dominant slip system due to high pressure [*Couvy et al.*, 2004; *Mainprice et al.*, 2005].

[34] The dominant activation of the (010)[001] slip system would result in the development of an orthorhombic LPO with [001] close to the lineation and [010] close to the foliation pole rather than a [010]-fiber pattern as observed in the Kerguelen xenoliths. Moreover, in the Kerguelen xenoliths,

orthopyroxene LPO show the same tendency as olivine LPO, i.e., a strong concentration of (100), the slip plane and a dispersion of [001], the slip direction; such a correlation is regarded as a strong argument supporting a transpressional strain regime shear [*Wenk et al.*, 1991; *Tommasi et al.*, 1999]. The role of pressure on the mechanical behavior of olivine is also excluded, the Kerguelen peridotite xenoliths being representative of a relatively shallow mantle (<70 km).

[35] We suggest that olivine LPO in Kerguelen harzburgite xenoliths results from a transpressional deformation of the lithospheric mantle under high-temperature and relative low-stress conditions. The simultaneous action of the asthenospheric upwelling due to the Kerguelen mantle plume and the emplacement of a very large oceanic plateau over a young oceanic lithosphere may induce a strain regime combining vertical flattening and simple shear accommodating the plate motion. Although there is yet no firm evidence of a relationship between the LPO pattern and the geographical location of the samples, harzburgites BY96-397 and GR97-38 that differ of the others ones by their orthorhombic olivine LPO, both come from the northern part of the Kerguelen Islands (Figure 1). The lithosphere under the northern part of Kerguelen Islands displays a specific fabric suggesting simple shear [*Tommasi et al.*, 1999], which may be due to the presence of deep fracture zones between the South East Indian Ridge and the Kerguelen plateau (e.g., transform faults) clearly visible on the satellite gravity maps [*Rotstein et al.*, 2001].

6.2. Melt-Rock Interactions, LPO, and Seismic Properties

[36] Partial melting, percolation and interaction of melts with the host mantle rocks are the processes that affect the lithospheric mantle above a mantle plume. For the Kerguelen lithospheric mantle, *Grégoire et al.* [1997] estimated a high degree (∼15–25 wt%) of partial melting, which created a depleted protogranular harzburgitic mantle. Petrological and geochemical studies support that the evolution from protogranular to poikilitic harzburgites and finally to dunites is the result of increasing metasomatism at higher melt/rock ratio and that this evolution leads to a global Fe-enrichment of minerals (olivine, orthopyroxene, clinopyroxene ± spinel). To better understand the effects of metasomatism on the LPO and therefore on the seismic properties, the relationship between the Mg# of olivine and the fabric strength (J index) as well as the seismic properties parameters (Vp, Vs, AVp and AVs) are investigated in Figure 12. Indeed, high J index values are observed for depleted protogranular harzburgites (J ∼ 12) characterized by high Mg# of olivine. The fabric strength is very sensitive to the onset of metasomatism at high melt/rock ratio, i.e., when the poikilitic microstructure starts to develop (Figure 12a), while J index decreases in poikilitic harzburgites and stabilizes in dunites. The crystallization of new olivine that is coupled with decreasing olivine Mg# induces a decrease of the fabric strength (Figure 12b).

[37] The relationship between seismic properties and metasomatism for harzburgites is not straightforward due to the variations in modal contents of olivine and orthopyroxene between the different samples. The results obtained for Kerguelen xenoliths are in general agreement with those obtained by *Tommasi et al.* [2004] for xenoliths from French Polynesia islands. For dunites, the velocity of P waves (Vp) appears to decreases with the Fe enrichment (decreasing Mg#) in olivine (Figure 12c). The velocity of P waves is higher for dunites (mainly > 8.45 km/s) than for harzburgites (<8.35 km/s) whereas the Vs average of dunites and harzburgites are very close, about 4.80 km/s for dunites and slightly higher for harzburgites (Figure 12d). The P wave velocity (Vp) is therefore more sensitive than Vs to Mg# variations. The seismic anisotropy (AVp and AVs) does not depend on Mg# variations but is mainly controlled by the LPO of minerals (Figures 12e and 12f). The calculated seismic anisotropies remain large (AVp > 5%) in spite of significant petrological and geochemical modifications of the original lithospheric mantle. A major difference with xenoliths from French Polynesia is that the geochemical and mineralogical changes induced by the harzburgite-silicate melt interactions, in particular the dissolution of orthopyroxene and crystallization of olivine, is coupled with a modification of the LPO pattern which results in contrasted seismic anisotropy distribution pattern (especially AVs) with regard to the crystallographic/structural referential (see seismic properties of harzburgites and dunites Figures 10b and 11b, respectively).

6.3. Seismic Anisotropy Beneath the Kerguelen Plateau

[38] Various seismic investigations have been performed on the Kerguelen plateau as follows: P and S waves seismic tomography revealed a wide and deep-rooted (from the core-mantle boundary) neg-

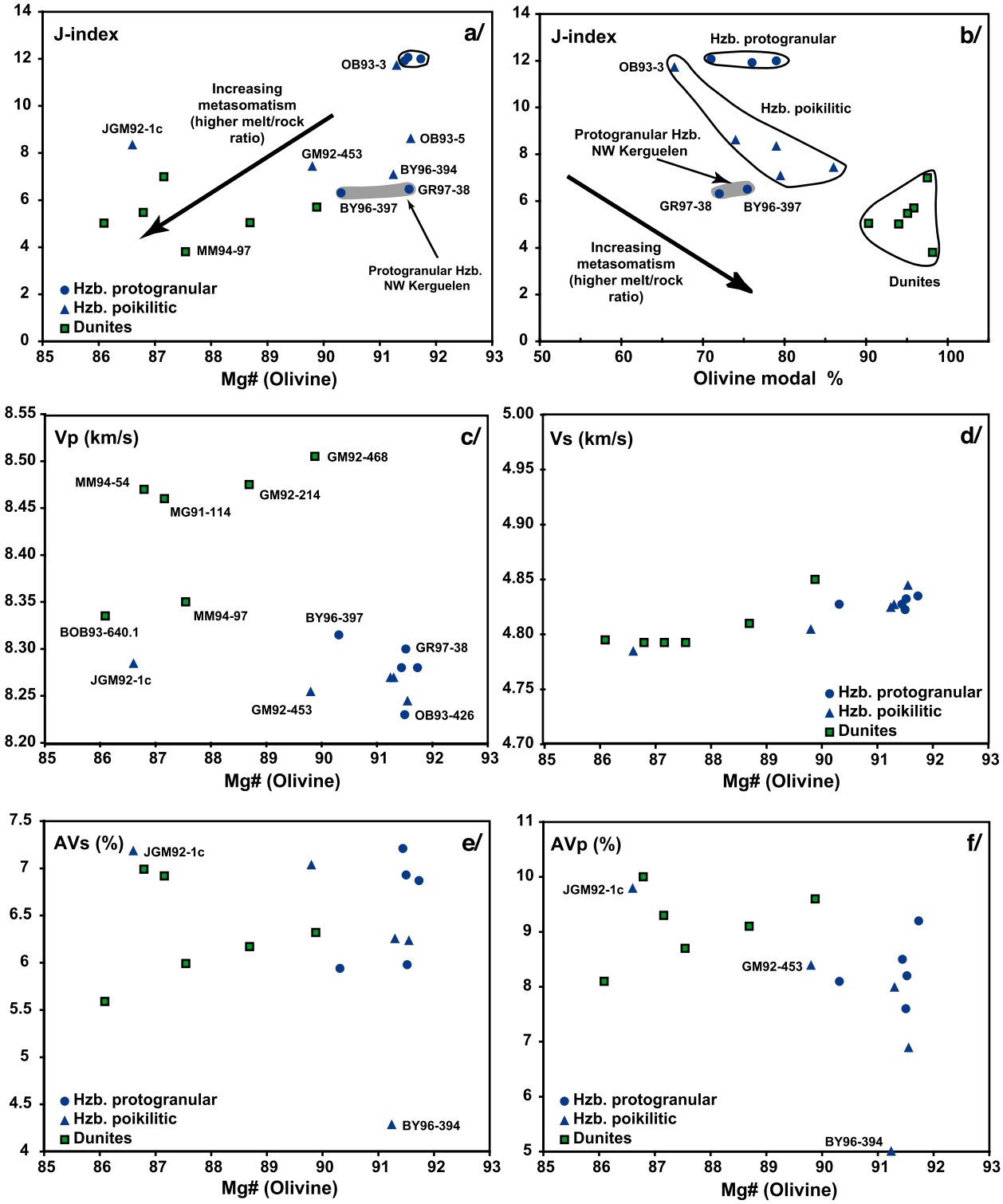

Figure 12. J index and seismic parameters (Vp (average), Vs (average), AVp and AVs) as a function of the mean forsterite content of olivine or modal olivine content in each sample.

ative velocity anomaly related to the Kerguelen (and Crozet) hot spots [*Montelli et al.*, 2006]. Seismic refraction and reflection profiles [*Recq et al.*, 1990; *Rotstein et al.*, 1992; *Charvis et al.*, 1995; *Operto and Charvis*, 1996] have evidenced an increase in crustal thickness from ~15–20 km beneath the northern Kerguelen Plateau (including the archipelago) to 25 km beneath the southern

plateau. Vp determinations for ultramafic and mafic xenoliths (deep-seated meta-igneous rocks) from the Kerguelen Archipelago by *Grégoire et al.* [2001] provide additional constraints on the seismic refraction profiles, and in particular the lithology of crust-mantle boundary.

[39] To characterize the mantle flow beneath the Kerguelen Islands, *Barruol and Hoffman* [1999] studied the seismic anisotropy of the mantle by measuring the splitting of teleseismic shear waves recorded at the Geoscope station *PAF* (Port aux Français, Figure 1) of Kerguelen. No clear splitting was observed but numerous ''nulls'' (unsplit core shear waves) were found for events from various backazimuths, suggesting apparent isotropy. By contrast, Rayleigh wave azimuthal anisotropy measurements [*Debayle et al.*, 2005] evidence a clear anisotropic pattern in the southern Indian Ocean at 100 km depth. Surface wave phase velocity studies of the Indian Ocean [*Lévêque et al.*, 1998] and of the Antarctic plate [*Roult et al.*, 1994] and surface wave polarization anomalies [*Pettersen and Maupin*, 2002] also argue for a rather strong anisotropy located in the 100 uppermost km beneath and in the vicinity of the Kerguelen Islands. Interestingly, results from surface wave data stand in better agreement with the seismic properties obtained from the Kerguelen xenoliths than S wave splitting measurements. Indeed, our results strongly suggest an anisotropic mantle beneath the Kerguelen Islands.

[40] To test the *Barruol and Hoffman* [1999] conclusions and discuss the causes of the discrepancy between core shear wave and surface wave anisotropies, we have reprocessed the whole data set recorded at PAF during the period 1993–2007 (Figure 13). About 700 events of magnitude (m_b) greater than 6.0 occurring at epicentral distances in the range 85° to 120° have been selected. The measurements were performed using the *Silver and Chan*'s [1991] algorithm and the SplitLab software [*Wüstefeld et al.*, 2008]. This new data set provided 26 non-null splitting measurements among which only one has been qualified as ''good'' (event occurring on February 7, 1997, backazimuth of 123°, ϕ = N93°, δt = 1.8 s). The others are close to nulls and are of lower quality. We also measured 90 ''nulls'' (no splitting) among which 66 are qualified as ''good'' and originate from a wide range of backazimuths. We conclude therefore that the updated S wave splitting measurements confirm the apparent isotropy proposed by *Barruol and Hoffman* [1999] for the PAF station. There is however a narrow azimuthal window in which the shear waves evidence an unambiguous splitting. This non-null splitting measurement among numerous nulls suggests a complex upper mantle structure beneath Kerguelen either due to multiple anisotropic layers or more likely to heterogeneity of mantle seismic properties. Dunites that show different seismic properties than harzburgites may carry a large part of the seismic heterogeneity above the Kerguelen mantle plume.

[41] The seismic core shear phases (SKS, SKKS...) propagate from the core-mantle boundary to the Earth's surface with a near vertical incidence. They therefore sample seismic properties of the anisotropic medium at rather steeply dipping incidence, i.e., within a rather limited cone. The measured delay time (δt) between the two split wave arrivals and, to lesser extent, the orientation of the fast split wave polarization plane (ϕ), besides being proportional to the thickness of the anisotropic medium, are dependent upon the characteristics and the orientation of its elastic tensor. This means that the observed anisotropy depends on the LPO of the rock-forming minerals and on the orientation of the structural reference frame (foliation, lineation), with respect to the vertical direction.

[42] The mantle xenoliths suite shows that the lithospheric mantle beneath Kerguelen Islands is primarily harzburgitic whereas the dunites probably represent restricted volumes of mantle rocks [*Grégoire et al.*, 1997]. Both protogranular and poikilitic harzburgites display [010]-fiber LPO pattern that induces specific seismic properties characterized by the lowest S wave polarization anisotropy (AVs) close to the pole of the foliation. Assuming that the lithospheric mantle beneath Kerguelen Archipelago is characterized by a dominant [010]-fiber texture and a penetrative horizontal foliation, the vertically propagating core shear waves arriving beneath the Kerguelen Archipelago would sample mantle in a direction for which it is apparently weakly anisotropic or even isotropic. This may explain the apparent isotropy revealed by the core S waves recorded at PAF. On the other hand, surface waves sample the mantle in a direction close or parallel to the foliation plane. The velocity of the Rayleigh waves would vary according to the propagation direction relative to the mantle fabric and an azimuthal anisotropy would be recorded. This may account for the clear azimuthal anisotropy observed at 100 km depth in Rayleigh wave tomography [e.g., *Debayle et al.*,

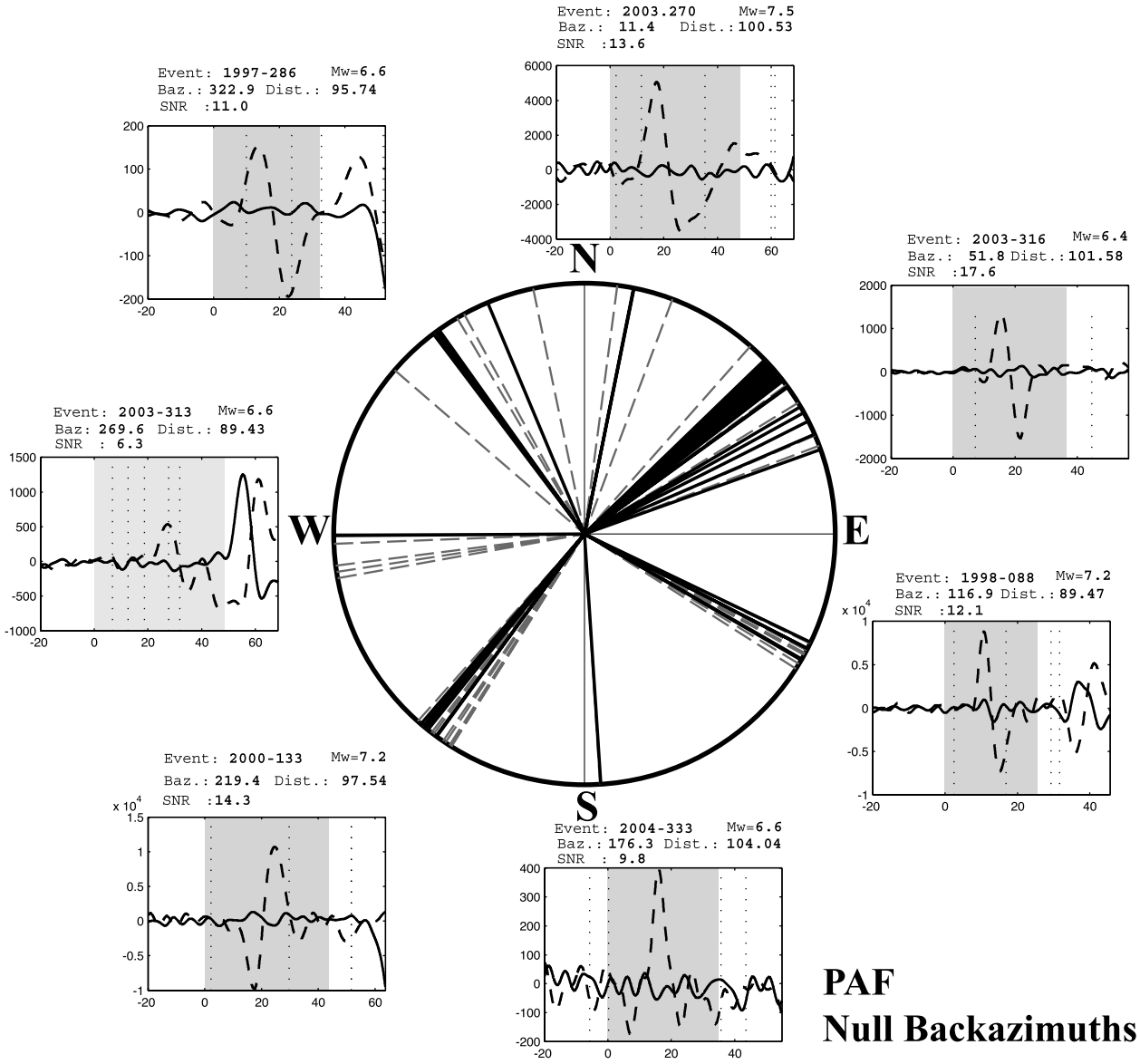

Figure 13. "Null" backazimuths observed at the Geoscope station PAF. Analysis of SKS data from 1993 to 2007 provided about 100 unsplit SKS phases arriving from a large range of backazimuths, suggesting that the upper mantle beneath the station is isotropic to the vertically propagating shear waves. This diagram displays the backazimuths of the events showing unsplit phases (black indicate good quality nulls, and dashed gray lines represent the fair quality nulls). Surrounding are a few examples of unsplit SKS phases. The radial (dashed line) and transverse (black line) components of the SKS phases are shown. For each event the magnitude (Mw), backazimuth (Baz, in degrees from north), epicentral distance (Dist., in degrees), and signal-to-noise ratio of the radial SKS phase are indicated.

2005] in the southern Indian Ocean around Kerguelen. If one considers a lithospheric mantle beneath Kerguelen structured with the foliation to be close to horizontal, what is expected in the lithospheric mantle and uppermost asthenosphere beneath a moving oceanic plate [e.g., *Forsyth*, 1975; *Nicolas and Christensen*, 1987], the independent isotropic SKS and anisotropic surface wave seismological observations appear therefore fully consistent together with the seismic properties computed for the Kerguelen xenoliths.

7. Conclusion

[43] Mantle xenoliths from the Kerguelen Islands represent various degrees of rock-melt interaction as supported by petrologic and geochemical studies. In particular, the Mg content in olivine decreases from protogranular to poikilitic harzbur-

gite and finally to dunite, which represents the ultimate stage of metasomatism. This process is correlated in harzburgite with a decrease in crystallographic fabric strength (J index is around 12 in most protogranular harzburgites and decreases down to 6.3 in poikilitic harzburgites). Dunites are affected by static recrystallization, which also weakens the fabric strength without however erasing it completely (J index $\geq$ 3.8). Lattice preferred orientation of olivine in harzburgites is characterized by a [010]-fiber pattern with strong concentration of [010] perpendicular to the foliation and by [100] distributed in the foliation plane with a maximum concentration close to the lineation. This olivine LPO is interpreted as due to a transpressional deformation regime resulting from a combination of simple shear accommodating the plate motion with vertical forces due to both the buoyancy of the mantle plume and the weight of the oceanic plateau. Olivine LPO in dunites is characterized by orthorhombic symmetry with high concentrations of [100] axes parallel to the lineation and [010] axes perpendicular to the foliation plane. From a seismic point of view, metasomatic processes at high melt/rock ratios result in a decrease of P wave velocities. The most significant difference between the Kerguelen harzburgites and dunites concerns the distribution of S wave splitting. Harzburgites display directions of high birefringence within the foliation plane and directions of minimum birefringence normal to the foliation plane, whereas the lowest birefringence is parallel to the lineation for dunites. This may have two consequences:

[44] 1. Assuming that harzburgites are representative of the initial composition of the lithosphere and that the foliation and lineation are subhorizontal, SKS splitting measurements may enhance an apparent isotropy while surface waves may support a significant anisotropy in the upper mantle. This may reconcile the apparent isotropy suggested by SKS wave splitting measurements for stations located on various Indian Ocean Islands, for instance Kerguelen, Crozet or New Amsterdam and the rather high anisotropy evidenced in the southern Indian Ocean using surface waves.

[45] 2. If the consequence of the metasomatism on the seismic properties of the mantle is at a scale significant for seismic waves, then this may result in a modification of the apparent anisotropy deduced from S waves splitting. Heterogeneous results at the regional scale might arise from such an evolution.

[46] Finally, beneath the Kerguelen Islands, lithosphere-plume interaction resulted in significant modifications of the composition, microstructure, texture and seismic properties of the initial mantle. This likely increased the heterogeneity of the mantle. Regarding texture and seismic properties, it is noteworthy that these processes did not erase the initial LPO and seismic anisotropy of the mantle but entailed significant modifications that may represent interesting constraints to refine the interpretation of seismic data.

Acknowledgments

[47] We thank C. Perrache and C. Nevado for the thin sections and A. Tommasi for constructive discussion and support through a DyETI project of INSU-CNRS, M. Grégoire, G. Michon, and the other members of Geology Department of St-Etienne University for lecture on the manuscript and scientific dialog. This work benefited greatly from software developed by D. Mainprice to generate pole figures and calculate rock seismic properties. We thank for their support the French Polar Institute (IPEV). We thank also the GEOSCOPE network for the accessibility and the quality of their data. For the geochemical work at GEMOC, Macquarie University, we would like to thank T. Bradley for the polished thin sections, A. Sharma, S. Elhlou, and C. Lawson for assistance with the analytical work, and S. O'Reilly, W. Griffin, and N. Pearson for ever-ready advice, assistance, and discussion. Analytical work at GEMOC was carried out using instrumentation funded by ARC LIEF and DEST Systemic Infrastructure Grants and Macquarie University. Support for geochemical analyses was provided from an ARC Discovery Grant (S.Y.O'R and others), the GEMOC ARC National Key Centre, an ARC IREX Grant (S.Y.O'R and W. L. Griffin), a Macquarie University Postgraduate Research Grant (G.D.) and a Macquarie University International Postgraduate Scholarship (G.D.). This is publication 509 in the GEMOC ARC National Key Centre. The manuscript has benefited from constructive reviews by M. Savage and G. Lloyd and comments by the editor, P. Van Keken.

References

Abramson, E. H., M. Brown, L. J. Slutsky, and J. Zaug (1997), The elastic constants of San Carlos olivine up to 17 GPa, *J. Geophys. Res.*, *102*, 12,253–12,263, doi:10.1029/97JB00682.

Babuska, V., and M. Cara (1992), *Seismic Anisotropy in the Earth*, 217 pp., Kluwer Acad., Dordrecht, Netherlands.

Barruol, G., and W. Ben Ismaïl (2001), Upper mantle anisotropy beneath the African IRIS and Geoscope stations, *Geophys. J. Int.*, *146*, 549–561, doi:10.1046/j.0956-540x.2001.01481.x.

Barruol, G., and R. Hoffman (1999), Upper mantle anisotropy beneath the Geoscope stations, *J. Geophys. Res.*, *104*, 10,757–10,773, doi:10.1029/1999JB900033.

Ben Ismaïl, W., and D. Mainprice (1998), An olivine fabric database: An overview of upper mantle fabrics and seismic anisotropy, *Tectonophysics*, *296*, 145–157, doi:10.1016/S0040-1951(98)00141-3.

Boyd, F. R. (1989), Compositional distinction between oceanic and cratonic lithosphere, *Earth Planet. Sci. Lett.*, *96*, 15–26, doi:10.1016/0012-821X(89)90120-9.

Bunge, H. J. (1982), *Texture Analysis in Materials Sciences*, 593 pp., Butterworths, London.

Charvis, P., M. Recq, M. Operto, and D. Brefort (1995), Deep structure of the northern Kerguelen plateau and hot spot-related activity, *Geophys. J. Int.*, *122*, 899–924, doi:10.1111/j.1365-246X.1995.tb06845.x.

Coffin, M. F., and O. Eldhom (1994), Large igneous provinces: Crustal structure, dimensions, and external consequences, *Rev. Geophys.*, *32*, 1–36, doi:10.1029/93RG02508.

Coisy, P., and A. Nicolas (1978), Structure et géodynamique du manteau supérieur sous le Massif Central (France) d'après l'étude des enclaves des basaltes, *Bull. Mineral.*, *4*, 424–436.

Collins, M. D., and J. M. Brown (1998), Elasticity of an upper mantle clinopyroxene, *Phys. Chem. Miner.*, *26*, 7–13, doi:10.1007/s002690050156.

Couvy, H., D. J. Frost, F. Heidelbach, K. Nyilas, T. Ungár, S. Mackwell, and P. Cordier (2004), Shear deformation experiments of forsterite at 11 GPa-1400°C in the multianvil apparatus, *Eur. J. Mineral.*, *16*, 877–889, doi:10.1127/0935-1221/2004/0016-0877.

Crosson, R. S., and J. W. Lin (1971), Voigt and Reuss prediction of anisotropic elasticity of dunite, *J. Geophys. Res.*, *76*, 570–578, doi:10.1029/JB076i002p00570.

Debayle, E., B. L. N. Kennett, and K. Priestley (2005), Global azimuthal seismic anisotropy and the unique plate-motion deformation of Australia, *Nature*, *433*, 509–512, PubMed, doi:10.1038/nature03247.

Delpech, G., M. Grégoire, S. O'Reilly, J. Y. Cottin, B. N. Moine, G. Michon, and A. Giret (2004), Feldspar from carbonate rich silicate metasomatism in the shallow oceanic mantle under Kerguelen Islands (south Indian Ocean), *Lithos*, *75*, 209–237, doi:10.1016/j.lithos.2003.12.018.

Dick, H. J. B. (1989), Abyssal peridotites, very slow spreading ridges and ocean ridge magmatism, in *Magmatism in the Ocean Basins*, edited by A. D. Saunders and M. J. Norry, *Geol. Soc. Spec. Publ.*, *42*, 71–105.

Duffy, T. S., and M. T. Vaughan (1988), Elasticity of enstatite and its relationships to crystal structure, *J. Geophys. Res.*, *93*, 383–391, doi:10.1029/JB093iB01p00383.

Duncan, R. A. (2002), A time for construction of the Kerguelen plateau and Broken ridge, *J. Petrol.*, *43*, 1109–1119, doi:10.1093/petrology/43.7.1109.

Fontaine, F., G. Barruol, A. Tommasi, and G. H. R. Bokelmann (2007), Upper mantle flow beneath French Polynesia from shear wave-splitting, *Geophys. J. Int.*, *170*, 1262–1288, doi:10.1111/j.1365-246X.2007.03475.x.

Forsyth, D. W. (1975), The early structural evolution and anisotropy of the oceanic upper mantle, *Geophys. J. R. Astron. Soc.*, *43*, 103–162.

Gautier, I., D. Weis, J. P. Mennessier, J. P. Vidal, A. Giret, and M. Loubet (1990), Petrology and geochemistry of the Kerguelen Archipelagos basalts (south Indian Ocean): Evolution of the mantle sources from ridge to intraplate position, *Earth Planet. Sci. Lett.*, *100*, 59–76, doi:10.1016/0012-821X(90)90176-X.

Giret, A. (1993), Les étapes magmatiques de l'édification des îles Kerguelen, océan Indien, *Mem. Soc. Geol. Fr.*, *163*, 273–282.

Grégoire, M., J. P. Lorand, J. Y. Cottin, A. Giret, N. Mattielli, and D. Weis (1997), Xenoliths evidence for a refractory oceanic mantle percolated by basaltic melts beneath the Kerguelen archipelago, *Eur. J. Mineral.*, *9*, 1085–1100.

Grégoire, M., J. P. Lorand, S. O'Reilly, and J. Y. Cottin (2000a), Armacolite-bearing, Ti-rich metasomatism assemblages in harzburgitic xenoliths from the Kerguelen Islands: Implication for the oceanic mantle budget of high-field strength elements, *Geochim. Cosmochim. Acta*, *64*, 673–694, doi:10.1016/S0016-7037(99)00345-2.

Grégoire, M., B. N. Moine, S. Y. O'Reilly, J. Y. Cottin, and A. Giret (2000b), Trace element residence and partitioning in mantle xenoliths metasomatised by high alkaline silicate, *J. Petrol.*, *41*, 477–509, doi:10.1093/petrology/41.4.477.

Grégoire, M., I. Jackson, S. Y. O'Reilly, and J. Y. Cottin (2001), The lithospheric mantle beneath the Kerguelen Islands (Indian Ocean): Petrological and petrophysical characteristics of mantle mafic rock types and correlation with seismic profiles, *Contrib. Mineral. Petrol.*, *142*, 244–259.

Hammond, J. O. S., J.-M. Kendall, G. Rümpker, J. Wookey, N. Teanby, P. Joseph, T. Ryberg, and G. Stuart (2005), Upper mantle anisotropy beneath the Seychelles microcontinent, *J. Geophys. Res.*, *110*, B11401, doi:10.1029/2005JB003757.

Hassler, D. R. (1999), Plume-lithosphere interaction: geochemical evidence from upper mantle and lower crustal xenoliths from the Kerguelen Islands, Ph.D. thesis, 372 pp., Mass. Inst. of Technol., Cambridge.

Hauri, E. H., and S. E. Hart (1994), Constraints on melt migration from mantle plumes: A trace element study of peridotites xenoliths from Savai'i, Western Samoa, *J. Geophys. Res.*, *99*, 24,301–24,321, doi:10.1029/94JB01553.

Holtzman, B. K., D. L. Kohlstedt, M. E. Zimmerman, F. Heidelbach, T. Hiraga, and J. Hustoft (2003), Melt segregation and strain partitioning: Implication for seismic anisotropy and mantle flow, *Science*, *301*, 1227–1230, PubMed, doi:10.1126/science.1087132.

Jung, H., and S. Karato (2001), Water-induced fabric transitions in olivine, *Science*, *293*, 1460–1463, PubMed, doi:10.1126/science.1062235.

Kaminski, E. (2006), Interpretation of seismic anisotropy in terms of mantle flow when melt is present, *Geophys. Res. Lett.*, *33*, L02304, doi:10.1029/2005GL024454.

Krieger Lassen, N. C. (1996), The relative precision of crystal orientations measured from electron backscattering patterns, *J. Microsc.*, *181*, 72–81.

Le Roux, V., J.-L. Bodinier, A. Tommasi, O. Alard, J. M. Dautria, A. Vauchez, and A. J. V. Riches (2007), The Lherz spinel lherzolite: Refertilized rather than pristine mantle, *Earth Planet. Sci. Lett.*, *259*, 599–612, doi:10.1016/j.epsl.2007.05.026.

Lévêque, J. J., E. Debayle, and V. Maupin (1998), Anisotropy in the Indian ocean upper mantle from Rayleigh and Love waveform inversion, *Geophys. J. Int.*, *133*, 529–540, doi:10.1046/j.1365-246X.1998.00504.x.

Li, Z., S. K. Chan, F. A. Garner, and R. C. Bradt (1995), Elastic stability of high dose neutron irradiated spinel, *J. Nucl. Mater.*, *219*, 139–142, doi:10.1016/0022-3115(94)00387-4.

Maggi, A., E. Debayle, K. Priestley, and G. Barruol (2006), Azimuthal anisotropy of the Pacific region, *Earth Planet. Sci. Lett.*, *250*, 53–71, doi:10.1016/j.epsl.2006.07.010.

Mainprice, D. (1990), A FORTRAN program to calculate seismic anisotropy from the lattice preferred orientation of minerals, *Comput. Geosci.*, *16*, 385–393, doi:10.1016/0098-3004(90)90072-2.

Mainprice, D., G. Barruol, and W. Ben Ismaïl (2000), The seismic anisotropy of the Earth's mantle: From single crystal to polycrystal, in *Earth's Deep Interior: Mineral Physics and Tomography From the Atomic to the Global Scale*, *Geophys. Monogr. Ser*, vol. 117, edited by S. I. Karato, pp. 237–264, AGU, Washington, D. C.

Mainprice, D., A. Tommasi, H. Couvy, P. Cordier, and D. J. Frost (2005), Pressure sensitivity of olivine slip systems and seismic anisotropy of Earth's upper mantle, *Nature*, *433*, 731–733, PubMed, doi:10.1038/nature03266.

Mattielli, N., D. Weis, M. Grégoire, J. P. Mennessier, J. Y. Cottin, and A. Giret (1996), Kerguelen basic and ultrabasic xenoliths: Evidence for long-lived Kerguelen hot spot activity, *Lithos*, *37*, 261–280, doi:10.1016/0024-4937(95)00040-2.

McDonough, W. F., and S.-S. Sun (1995), The composition of the earth, *Chem. Geol.*, *120*, 223–253, doi:10.1016/0009-2541(94)00140-4.

Mercier, J.-C., and A. Nicolas (1975), Textures and fabrics of upper mantle peridotites as illustrated by xenoliths from basalts, *J. Petrol.*, *16*, 454–487.

Moine, B. N., M. Grégoire, S. Y. O'Reilly, S. M. F. Sheppard, and J. Y. Cottin (2001), High field strength element fractionation in the upper mantle: Evidence from amphibole-rich composite mantle xenolith from the Kerguelen Islands (Indian Ocean), *J. Petrol.*, *42*, 2145–2167, doi:10.1093/petrology/42.11.2145.

Moine, B. N., M. Grégoire, S. O'Reilly, G. Delpech, S. M. F. Sheppard, J. P. Lorand, C. Renac, A. Giret, and J. Y. Cottin (2004), Carbonatite melt on oceanic upper mantle beneath the Kerguelen Archipelagos, *Lithos*, *75*, 239–252, doi:10.1016/j.lithos.2003.12.019.

Montagner, J. P., and T. Tanimoto (1991), Global upper mantle tomography of seismic velocities and anisotropies, *J. Geophys. Res.*, *96*, 20,337–20,351, doi:10.1029/91JB01890.

Montelli, R., G. Nolet, F. A. Dahlen, and G. Masters (2006), A catalog of deep mantle plumes: New results from finite-frequency tomography, *Geochem. Geophys. Geosyst.*, *7*, Q11007, doi:10.1029/2006GC001248.

Nazé, L., N. Doukhan, J. C. Doukhan, and K. Latrous (1987), TEM study of lattice defects in naturally and experimentally deformed orthopyroxenes, *Bull. Mineral.*, *110*, 497–512.

Nicolas, A., and N. I. Christensen (1987), Formation of anisotropy in upper mantle peridotites — A review, in *Composition, Structure and Dynamics of the Lithosphere-Asthenosphere System*, *Geodyn. Ser*, vol. 16, edited by K. Fuchs and C. Froidevaux, pp. 111–123, AGU, Washington, D. C.

Nicolas, A., and J. P. Poirier (1976), *Crystalline Plasticity and Solid State Flow in Metamorphic Rocks*, 444 pp., John Wiley, New York.

Nicolaysen, K., F. A. Frey, K. V. Hodges, D. Weis, and A. Giret (2000), $^{40}Ar/^{39}Ar$ geochronology of flood basalts from the Kerguelen Archipelago, southern Indian Ocean: Implications for Cenozoic eruption rates of the Kerguelen plume, *Earth Planet. Sci. Lett.*, *174*, 313–328, doi:10.1016/S0012-821X(99)00271-X.

Operto, M., and P. Charvis (1996), Deep structure of the southern Kerguelen Plateau (southern Indian Ocean) from ocean bottom ocean bottom seismometer wide-angle seismic data, *J. Geophys. Res.*, *101*, 25,077–25,103, doi:10.1029/96JB01758.

Pettersen, O., and V. Maupin (2002), Lithospheric anisotropy on the Kerguelen hot spot track inferred from Rayleigh wave polarization anomalies, *Geophys. J. Int.*, *149*, 225–246, doi:10.1046/j.1365-246X.2002.01646.x.

Recq, M., D. Bredfort, J. Malod, and J. L. Veinante (1990), The Kerguelen Isles (southern Indian Ocean): New results on deep structure from refraction profiles, *Tectonophysics*, *182*, 227–248, doi:10.1016/0040-1951(90)90165-5.

Rotstein, Y., R. Schlich, and M. Munschy (1992), Structure and tectonic of the southern Kerguelen plateau (Indian Ocean) deduced from reflection data, *Tectonics*, *11*, 1332–1347, doi:10.1029/91TC02909.

Rotstein, Y., M. Munschy, and A. Bernard (2001), The Kerguelen Province revisited: Additional constraints on the early development of the southeast Indian Ocean, *Mar. Geophys. Res.*, *22*, 81–100, doi:10.1023/A:1010345608833.

Roult, G., D. Rouland, and J. P. Montagner (1994), Antarctica II: Upper-mantle structure from velocities and anisotropy, *Phys Earth Planet Inter*, *84*, 33–57, doi:10.1016/0031-9201(94)90033-7.

Russo, R., and E. Okal (1998), Shear wave splitting and upper mantle deformation in French Polynesia: Evidence for small-scale heterogeneity related to the Society hot spot, *J. Geophys. Res.*, *103*, 15,089–15,107, doi:10.1029/98JB01075.

Schmidt, N. H., and N. Ø. Olesen (1989), Computer-aided determination of crystal-lattice orientation from electron-channeling patterns in the SEM, *Can. Mineral.*, *27*, 15–22.

Silver, P. G. (1996), Seismic anisotropy beneath the continents: Probing the depths of geology, *Annu. Rev. Earth Planet. Sci.*, *24*, 385–432, doi:10.1146/annurev.earth.24.1.385.

Silver, P. G., and W. W. Chan (1991), Shear wave splitting and subcontinental mantle deformation, *J. Geophys. Res.*, *96*, 16,429–16,454, doi:10.1029/91JB00899.

Tommasi, A., B. Tikoff, and A. Vauchez (1999), Upper mantle tectonics: Three-dimensional deformation, olivine crystallographic fabrics and seismic properties, *Earth Planet. Sci. Lett.*, *168*, 173–186, doi:10.1016/S0012-821X(99)00046-1.

Tommasi, A., M. Godard, G. Coromina, J. M. Dautria, and H. Barsczus (2004), Seismic anisotropy and compositionally induced velocity anomalies in the lithosphere above mantle plumes: A petrological and microstructural study of mantle xenoliths from French Polynesia, *Earth Planet. Sci. Lett.*, *227*, 539–556, doi:10.1016/j.epsl.2004.09.019.

Vauchez, A., and C. J. Garrido (2001), Seismic properties of an asthenospherized lithospheric mantle: Constraints from lattice preferred orientations in peridotite from the Ronda Massif, *Earth Planet. Sci. Lett.*, *192*, 235–249, doi:10.1016/S0012-821X(01)00448-4.

Vauchez, A., F. Dineur, and R. Rudnick (2005), Microstructure, texture and seismic anisotropy of the lithospheric mantle above a mantle plume: Insights from the Labait volcano xenoliths (Tanzania), *Earth Planet. Sci. Lett.*, *232*, 295–314, doi:10.1016/j.epsl.2005.01.024.

Vollmer, F. W. (1990), An application of eigenvalue methods to structural domain analysis, *Geol. Soc. Am. Bull.*, *102*, 786–791, doi:10.1130/0016-7606(1990)102<0786:AAOEMT>2.3.CO;2.

Wenk, H-.R., K. Bennet, G. R. Canova, and A. Molinari (1991), Modeling plastic deformation of peridotite with the self-consistent theory, *J. Geophys. Res.*, *96*, 8337–8349, doi:10.1029/91JB00117.

Wolfe, C., and P. G. Silver (1998), Seismic anisotropy of oceanic upper mantle: Shear wave splitting methodologies and observations, *J. Geophys. Res.*, *103*, 749–771, doi:10.1029/97JB02023.

Wulff-Pedersen, E., E.-R. Neumann, and B. B. Jensen (1996), The upper mantle under La Palma, Canary Islands: Formation of Si-K-Na-rich melt and its importance as a metasomatic agent, *Contrib. Mineral. Petrol.*, *125*, 113–139, doi:10.1007/s004100050210.

Wüstefeld, A., G. H. R. Bokelmann, C. Zaroli, and G. Barruol (2008), SplitLab: A shear wave splitting environment in Matlab, *Comput. Geosci.*, *34*, 515–528, doi:10.1016/j.cageo.2007.08.002.